GEOLOGICAL SURVEY OF CANADA
OPEN FILE 7853

Targeted Geoscience Initiative 4: Contributions to the Understanding of Volcanogenic Massive Sulphide Deposit Genesis and Exploration Methods Development

Major ore types of the Paleoproterozoic Lalor auriferous volcanogenic massive sulphide deposit, Snow Lake, Manitoba

Shamus Duff[1], Mark D. Hannington[1], Antoine Caté[2], Patrick Mercier-Langevin[3], and Ingrid M. Kjarsgaard[4]

[1]University of Ottawa, Ottawa, Ontario
[2]Institut national de la recherche scientifique, Québec, Quebec
[3]Geological Survey of Canada, Québec, Quebec
[4]Consulting Mineralogist, Ottawa, Ontario

2015

Recommended citation

Duff, S., Hannington, M.D., Caté, A., Mercier-Langevin, and Kjarsgaard, I.M., 2015. Major ore types of the Paleoproterozoic Lalor auriferous volcanogenic massive sulphide deposit, Snow Lake, Manitoba, *In:* Targeted Geoscience Initiative 4: Contributions to the Understanding of Volcanogenic Massive Sulphide Deposit Genesis and Exploration Methods Development, (ed.) J.M. Peter and P. Mercier-Langevin; Geological Survey of Canada, Open File 7853, p. 147–170.

Publications in this series have not been edited; they are released as submitted by the author.

Contribution to the Geological Survey of Canada's Targeted Geoscience Initiative 4 (TGI-4) Program (2010–2015)

TABLE OF CONTENTS

Figures

Tables

Major ore types of the Paleoproterozoic Lalor auriferous volcanogenic massive sulphide deposit, Snow Lake, Manitoba

Shamus Duff[1,*], Mark D. Hannington[1†], Antoine Caté[2], Patrick Mercier-Langevin[3], and Ingrid M. Kjarsgaard[4]

[1]Department of Earth Sciences, University of Ottawa, Ottawa, Ontario K1N 6N5
[1]Institut national de la recherche scientifique, 490 rue de la Couronne, Québec, Quebec G1K 9A9
[2]Geological Survey of Canada, 490 rue de la Couronne, Québec, Quebec G1K 9A9
[4]Consulting Mineralogist, 15 Scotia Place, Ottawa, Ontario K1S 0W2
*Corresponding author's e-mail: sduff088@uottawa.ca
†Corresponding author's e-mail: mark.hannington@uottawa.ca

ABSTRACT

The Lalor deposit is a newly discovered Paleoproterozoic volcanogenic massive sulphide (VMS) deposit located at the east end of the Flin Flon-Snow Lake belt, within the Snow Lake arc assemblage. Lalor is the largest of 11 VMS deposits in the Snow Lake arc assemblage, with combined resources and reserves of 25.3 Mt and average grades of 2.9 g/t Au, 25 g/t Ag, 5 wt% Zn, and 0.79 wt% Cu, including 8.8 Mt at 4.6 g/t Au. Lalor and all other deposits in the Snow Lake arc assemblage have been affected by intense polyphase deformation and amphibolite facies metamorphism. As a result, both the original hydrothermal alteration assemblages and the ore mineral assemblages have been completely recrystallized. However, a variety of different ore types have been preserved, allowing the partial reconstruction of the hydrothermal system, including massive Fe-Zn sulphide lenses, discordant Cu-Au stringer zones, and distinctive precious metal-rich Au-Ag-Pb-Cu zones. The different ore types occur in a series of stratigraphically and structurally "stacked" ore lenses that partly overlap but still largely preserve the original architecture of the deposit.

The ore is distributed in 12 discrete lenses or zones of mineralization that are interpreted to be the result of several distinct and overlapping hydrothermal events. Type 1 Fe-Zn massive sulphide ore is the most common ore type in 6 ore lenses and consists of massive coarse-grained pyrite and sphalerite with trace galena in dominantly quartz-muscovite±kyanite-biotite schist (K-alteration association). Type 2 Cu-Au mineralization consists of semi-massive and stockwork chalcopyrite and pyrrhotite in garnetiferous quartz-biotite±staurolite-amphibole-cordierite gneisses (footwall Mg-Fe alteration association). Despite extensive recrystallization and local remobilization, these two ore types are interpreted to represent the (metamorphosed) low- and high-temperature ore assemblages, respectively, of a typical volcanogenic massive sulphide deposit. Type 3 Au-Ag-Pb-Cu-rich ore consists of stringer and disseminated sulphides and sulphosalts mainly hosted in chlorite-carbonate-actinolite schist (Mg-Ca and Ca alteration associations). Galena is an important indicator of Au mineralization and occurs in this ore type as fine-grained blebs in a matrix of chlorite, dolomite, calcite, anthophyllite, Ca-plagioclase, and calc-silicates (epidote, grossular, diopside, Ca-amphibole ± scapolite). Where abundant, the galena is associated with chalcopyrite, pyrite, and pyrrhotite, and with minor to trace sphalerite, Ag-Sb-Pb sulphosalts, electrum, and native gold. Type 4 low-sulphide ore contains ≤10 vol% disseminated pyrite in quartz-biotite-anthophyllite gneiss, with minor chlorite, staurolite, and coarse almandine garnet, and has variable Au grades. The sulphides and sulphosalts in ore types 3 and 4 are interpreted to be metamorphically remobilized from pre-existing disseminated mineralization.

The hydrothermal system developed during two main episodes of seafloor volcanism. Type 1 massive sulphide in the 10 and 11 lenses and in the 20, 30, 31, and 40 lenses were formed at the paleoseafloor. These lenses are underlain by Type 2 Cu-Au stockwork mineralization (27 Lens) and originally conformable zones of Type 3 Au-Ag-Pb mineralization (21, 24, 25, 26, and 28 lenses). The large Cu-Au stockwork zone (27 Lens) may have been the main feeder of the deposit and is partly continuous with disseminated Au-Ag-Pb-Cu galena-sulphosalts-chalcopyrite mineralization below the 20 Lens. The Au-Ag-Pb-Cu mineralization is thought to have formed in the subseafloor from late-stage, lower temperature hydrothermal fluids (approximately <300°C). In this model, significant Au was introduced first by high-temperature (>300°C) fluids responsible for the Type 2 Cu-Au mineralization and then by lower temperature (possibly boiling) hydrothermal fluids responsible for Type 3 Ag-Au-Pb-Cu mineralization. Although all the ore types are extensively recrystallized and partly remobilized, their distribution strongly supports primary hydrothermal

Duff, S., Hannington, M.D., Caté, A., Mercier-Langevin, and Kjarsgaard, I.M., 2015. Major ore types of the Paleoproterozoic Lalor auriferous volcanogenic massive sulphide deposit, Snow Lake, Manitoba, *In:* Targeted Geoscience Initiative 4: Contributions to the Understanding of Volcanogenic Massive Sulphide Deposit Genesis and Exploration Methods Development, (ed.) J.M. Peter and P. Mercier-Langevin; Geological Survey of Canada, Open File 7853, p. 147–170.

Au enrichment at Lalor. The lead isotopic compositions of the ore galena show no evidence of post-magmatic disturbance, which would be expected if Au had been introduced during deformation and metamorphism (e.g. as in the nearby New Britannia orogenic Au deposit), and the Au-rich assemblages are very similar to those that commonly occur in unmetamorphosed Au-rich volcanogenic massive sulphide deposits.

INTRODUCTION

The Lalor volcanogenic massive sulphide (VMS) deposit is located in Snow Lake, Manitoba, 200 km east of the Flin Flon and 777 deposits. The Snow Lake camp has been a prolific producer of base metals and Au since 1949, with more than 10 past-producing VMS deposits (Table 1) as well as the closed New Britannia (formerly Nor Acme) orogenic Au mine. Lalor is the largest VMS deposit to have been put into production in Snow Lake and the only currently operating mine in the area. The combined resources and reserves total 25.3 Mt with grades of 2.9 g/t Au, 25 g/t Ag, 5 wt% Zn and 0.79 wt% Cu (HudBay Minerals Inc., 2014), including 8.8 Mt at 4.6 g/t Au, making it the largest and richest VMS deposit of the Snow Lake camp (Mercier-Langevin et al., 2014). The Au grades are among the highest of any deposit in the Flin Flon-Snow Lake belt, rivalling those of the nearby Chisel North and Photo Lake auriferous VMS deposits (e.g. Galley et al., 2007). This paper describes the main ore lenses of the Lalor deposit and the spatial and paragenetic relationships of the different ore types, with the aim of better constraining the Au-enrichment processes and their relative timing.

REGIONAL AND DEPOSIT GEOLOGY

The 10 past-producing VMS mines in the Snow Lake district (Rod, Stall, Anderson, Ghost, Chisel, Chisel North, Photo Lake, Osborne Lake, Reed Lake, and Spruce Point) and the currently operating Lalor Mine are located in the Snow Lake arc assemblage (SLA; Fig. 1). The Lalor deposit is in the lower portion of the Chisel sequence (termed Lower Chisel subsequence), together with the Chisel, Lost, and Ghost Zn-Cu deposits and the Photo Lake auriferous VMS deposit (Fig. 2; Bailes and Galley, 1999; Bailes, 2009; Bailes et al., 2013; Caté et al., 2014; Engelbert et al., 2014a,b). The Lower Chisel subsequence consists of bimodal mafic and felsic volcanic rocks, dominated by mafic volcaniclastic rocks and aphyric basalt and the Powderhouse dacite unit. These rocks are overlain by the Threesomes basalt (Galley et al., 2007), which marks the transition between the lower and upper parts of the Chisel sequence (Bailes and Galley, 1996; Engelbert, et al., 2014a,b). The Chisel and Chisel North deposits are spatially associated with rhyolite domes, located close to the contact between the Upper and Lower Chisel subsequences (Galley et al., 1993; Bailes and Galley, 1996; Bailes, 2009). The Anderson sequence, which underlies the Chisel sequence and hosts the Stall, Rod, and Anderson deposits, consists dominantly of aphyric basalt and small felsic centres. In contrast to the deposits of the Chisel sequence, which are dominantly Zn-Cu deposits, the deposits of the Anderson sequence are distinctly Cu-rich (Bailes et al., 2013).

Table 1. Grades and tonnage of current and past-producing volcanogenic massive sulphide deposits of Snow Lake (after Bailes et al., 2013).

Mine	Tonnes	Au (g/t)	Ag (g/t)	Cu (wt%)	Zn (wt%)
Chisel Sequence					
Lalor Zn-Cu	18100000	0.64	25.24	0.64	8.97
Lalor Cu-Au	5400000	4.7	30.6	0.47	0.46
Chisel	7153532	1.76	44.76	0.54	10.6
Chisel North	2606212	0.58	21.43	0.21	9.49
Ghost and Lost	581438	1.2	39.09	1.34	8.6
Photo Lake	689885	4.9	29.38	4.58	6.35
Anderson Sequence					
Stall	6381129	1.41	12.34	4.41	0.5
Rod	735219	1.71	16.11	6.63	2.9
Anderson	2510000	0.62	7.54	3.4	0.1
Other					
Schist Lake	1846656	1.3	37.03	4.3	7.27
Osborne	2807471	0.27	4.11	3.14	1.5
Spruce Point	1865095	1.68	19.54	2.06	2.4
Reed Lake	2720000	0.62	7.63	4.5	0.89

The Snow Lake arc assemblage is affected by at least four episodes of deformation associated with the Trans-Hudson orogeny (Kraus and Williams, 1999). The D_1 and D_2 events produced tight, isoclinal, south-verging folds, shallowly dipping thrusts, and the main foliation (Kraus and Williams, 1999; Bailes et al., 2013). These structures are refolded by north-north-east-trending F_3 folds and an associated S_3 crenulation cleavage (Martin, 1966; Kraus and Williams, 1999). The F_4 folds with east-trending axes locally overprint F_3 folds (Kraus and Williams, 1999). In the Lalor deposit, $D_{1\text{-}2}$ and D_3 structures largely control the geometry of the ore lenses (Caté et al., 2014a). Volcanic units in the host succession are generally oriented parallel to the main $S_{1\text{-}2}$ foliation and dip to the northeast (Caté et al., 2014a). The hanging-wall rocks are part of a separate volcanic succession in structural contact with the Lalor volcanic succession (Caté et al., 2014b) that dips steeply toward the northeast (Bailes, 2008, 2011).

The ore lenses of the Lalor deposit are located in the uppermost section of a volcanic succession that has

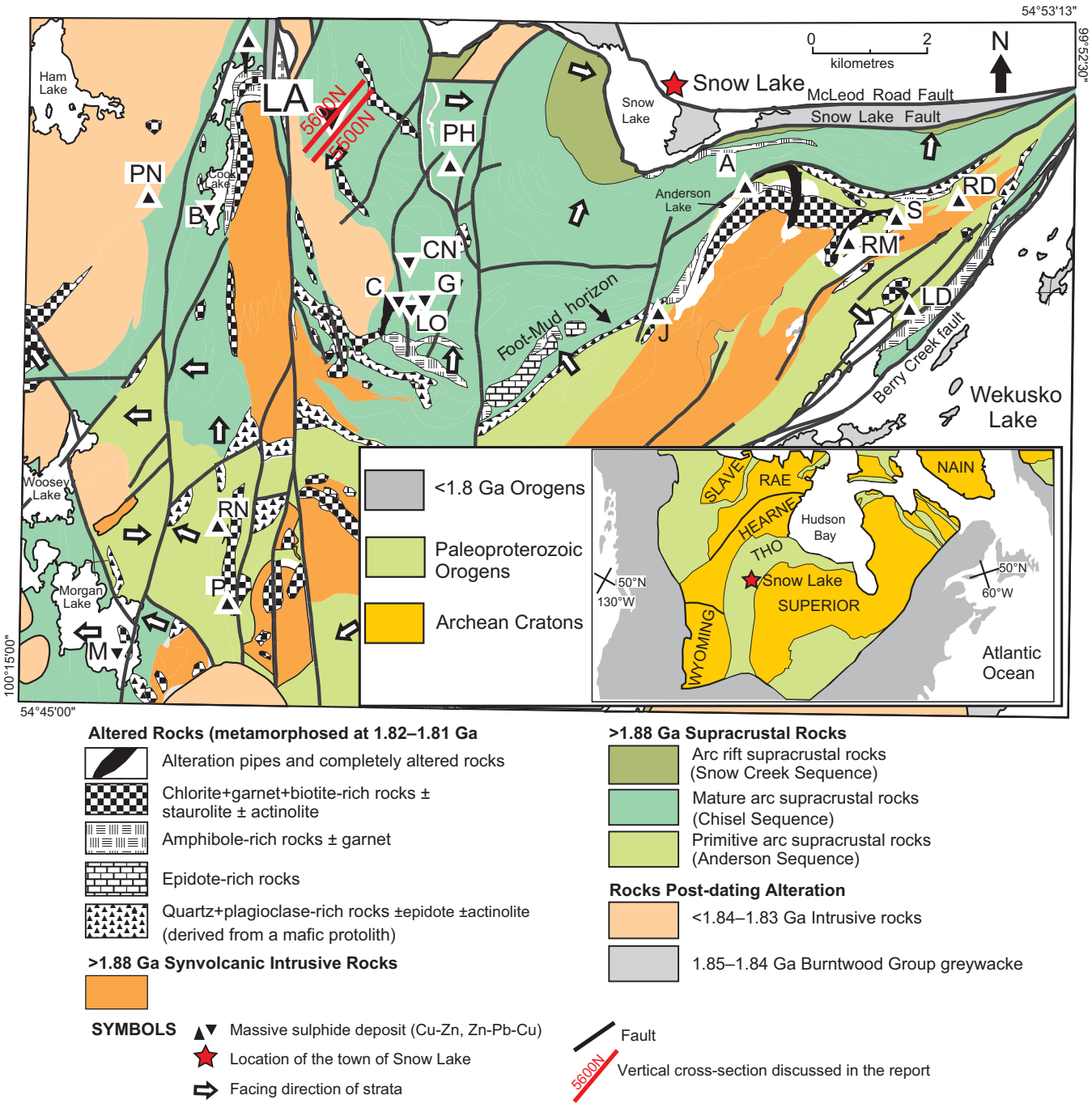

Figure 1. Simplified geological map of the Snow Lake area (from Galley et al., 2007), showing major alteration zones and volcanogenic massive sulphide deposits, including the Lalor deposit (LA). Other deposits: A = Anderson; B = Bomber zone; C = Chisel Lake; CN = Chisel North; G = Ghost; J = Joannie zone; LO = Lost; LD = Linda zone; M = Morgan Lake zone; P = Pot Lake zone; PH = Photo Lake; PN = Pen zone; RD = Rod; RM = Ram zone; RN = Raindrop zone; S = Stall Lake. The location of the Snow Lake area in North America is shown in the inset map.

been intensely hydrothermally altered (Lalor volcanic succession: Caté et al., 2014b). The hydrothermal alteration was metamorphosed to amphibolite facies during D_{1-2}, with syn- to late-D_2 peak conditions estimated at ~5 kbar and temperatures up to 550°C (Zaleski et al., 1991; Menard and Gordon, 1997; Lam et al., 2013, 2014; Tinkham, 2013). The metamorphic mineral assemblages have been correlated with whole-rock lithogeochemistry and define 5 distinct chemical associations (K-rich, K-Fe-Mg, Mg-Fe, Mg-Ca, and Ca) described by Caté et al. (2013a,b, 2015).

SAMPLING AND ANALYTICAL METHODS

In June through August 2012, 11 exploration drillholes along section 5600 N were logged and sampled in detail (Fig. 3). The drill core was logged in the interval

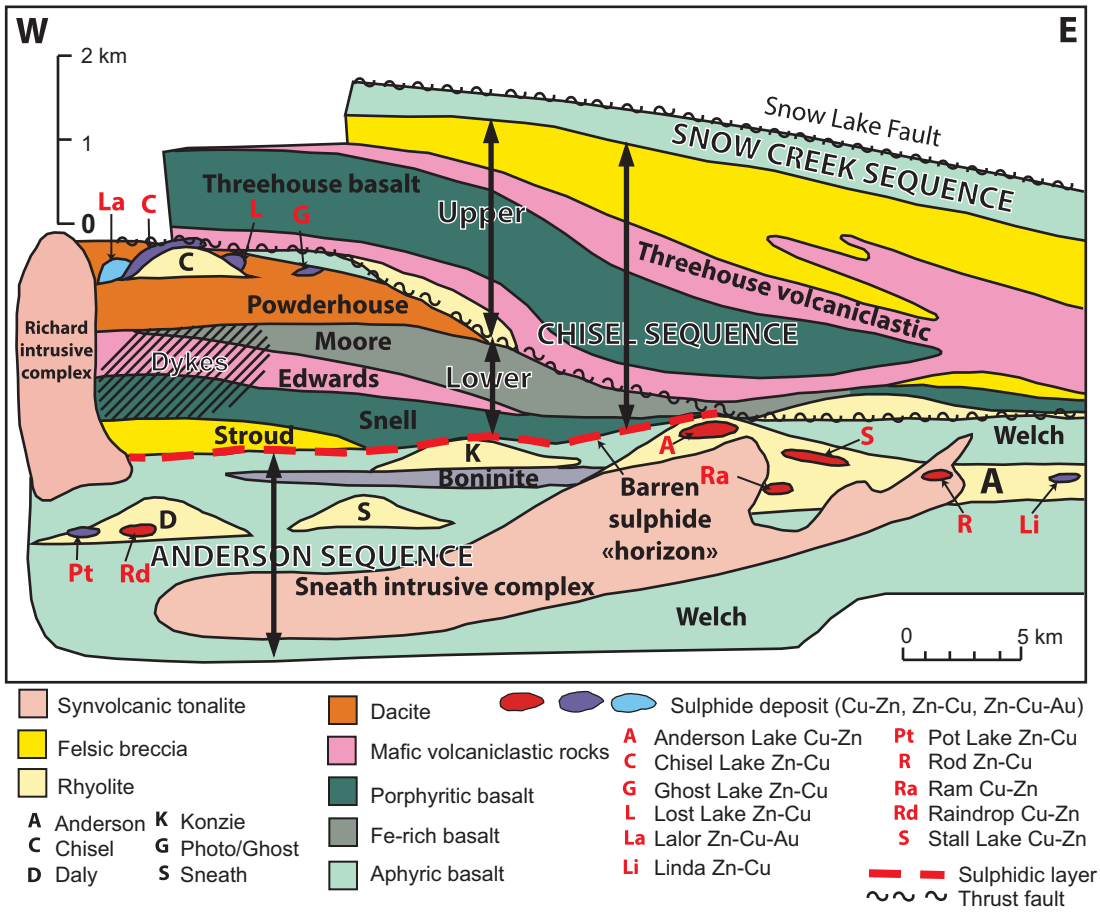

Figure 2. Schematic cross-section through the Snow Lake arc assemblage (Bailes et al., 2013, modified from Bailes and Galley, 1999), showing the positions of the Lalor, Chisel, Lost, and Ghost Zn-Cu deposits and the Photo Lake Au-rich volcanogenic massive sulphide deposit in the upper portion of the Chisel Sequence.

starting 50 m above the first sign of significant mineralization to the end of the hole. Samples were collected wherever strong mineralization was intersected, with the aim of encompassing the entire deposit and obtaining representative samples of all the different ore types. An additional 10 exploration holes were logged along section 5300 N. All logging and sampling was completed between May and August 2013. During this time, the mine opened and was in a pre-production phase, allowing the opportunity to map and sample underground in 5 areas between 795 and 865 m below surface. Results of the underground mapping and sampling are presented in Caté et al. (2014a, 2015).

Seventy drill-core samples were selected for detailed petrographic study and chemical analysis, including major metals, oxides, and trace elements. Splits of each sample were crushed using a steel jaw crusher (in order to increase Au content and minimize cross-contamination), then pulverized in a Cr-steel mill, both at the University of Ottawa. Pulverized samples were analyzed at Activation Laboratories in Ancaster, Ontario. SiO_2, Al_2O_3, Fe_2O_3, MnO, MgO, CaO, Na_2O, K_2O, TiO_2, P_2O_5, Sc, Be, V, Sr, and Ba were analyzed by peroxide fusion followed by dissolution and inductively couple plasma optical emission spectrometry (FUS-ICPOES). Silver, As, Bi, Ce, Co, Cr, Cu, Dy, Er, Eu, Ga, Gd, Ge, Hf, Ho, In, La, Lu, Mo, Nb, Nd, Ni, Pb, Pr, Rb, Sb, Sm, Sn, Tb, Tm, Ta, Tl, Th, U, W, Y, Yb, and Zr were analyzed by fusion followed by ICP mass spectrometry (FUS-ICPMS). Silver, Cd, Co, Cr, Cu, In, Li, Mn, Mo, Ni, Pb, and Zn were analyzed by 4-acid total dissolution followed by ICP mass spectrometry (TD-ICPMS). Tellurium, Se, As, Bi, and Sb were analyzed by hydride generation and ICPMS, and Hg was analyzed on a flow injection mercury system (Hg-FIMS). Gold and Ag were analyzed by fire assay with a graphite-furnace atomic absorption finish. Fluorine was analyzed by specific ion electrode, and B was analyzed by prompt gamma neutron activation analysis (PGNAA). Total C, S, and CO_2 were analyzed by combustion and infrared detection (IR). Loss on ignition was also determined by combustion. FeO was determined by titration. The full analytical data, including detections limits and reproducibility are included in the M.Sc. thesis of S. Duff (in prep.).

Petrographic descriptions of the main ore types were supplemented by microanalysis of representative ore minerals, and gangue by wavelength dispersive X-ray

a)

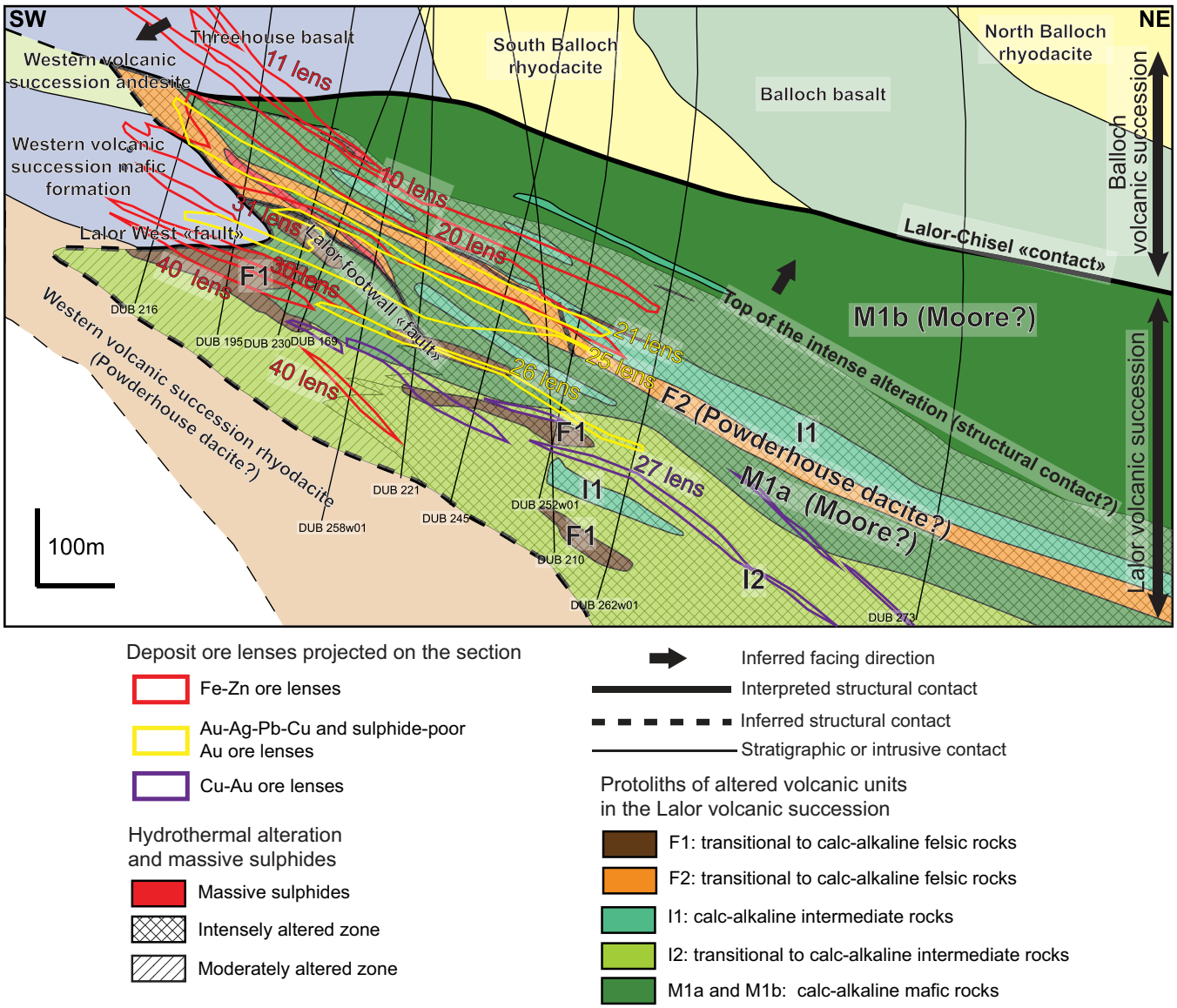

Figure 3. Schematic cross-section of the Lalor deposit at 5600 N (looking northwest) from Caté et al. (2014). The approximate locations of the main Fe-Zn massive sulphide, Au-Ag-Pb-rich ore zones, and Au-Cu zones discussed in the text are shown. 10 Lens is projected from section 5500 N. Inferred lithologies are from Caté et al. (2014) and (Bailes, 2008).

analysis (WDX) using a four-spectrometer Camebax MBX electron microprobe at the Earth Sciences Department of Carleton University, Ottawa. Sulphur isotope analyses were made on selected mineral separates of pyrite, chalcopyrite, pyrrhotite, sphalerite, and galena at the University of Ottawa's G.G. Hatch Stable Isotope Laboratory. Lead isotope ratios of galena were determined at Carleton University's Isotope Geochemistry and Geochronology Center (IGGC).

DISTRIBUTION OF THE ORE LENSES

Unlike other deposits in the Snow Lake camp, the ore at Lalor is distributed among many different lenses. The currently defined resource has been divided into 12 ore lenses. Assay data for the main lenses considered in this study are shown in Table 2. Some of the ore lenses (main massive sulphide lenses 10, 11, 20, 30, 31, and 40) are conformable with the host stratigraphy (dipping ~30°) and are stacked. The longest dimensions of most of these lenses strike northwest-southeast; however, the 20 Lens, in the middle of the succession, strikes north-south, possibly indicating an intersecting fault control. Although the 6 main massive sulphide lenses are stacked, Bailes (2011) and Caté et al. (2014, 2015) suggest that there are fewer primary ore horizons, and numerous thrust faults and/or folds are likely responsible for the dismemberment and "stacking" of multiple sulphide zones. They recognized only two paleoseafloor horizons, one containing the 10 and 11 lenses and the other hosting the 20, 30, 31, and 40 lenses (Bailes et al., 2013; Caté et al., 2014a,b). The lithogeochemically distinct rock types that host the

Table 2. Average ore grades of the different lenses discussed in the text (from Hudbay Minerals Inc.).

Lens	Ore Type	Au (g/t)	Ag (g/t)	Cu (wt%)	Zn (wt%)	Pb (wt%)	Fe (wt%)
Fe-Zn							
10	Type 1	2.12	23.58	0.79	11.48	0.25	25.28
11	Type 1	0.21	17.1	0.26	12.13	0.06	27.88
20	Type 1	2.49	31.16	0.91	8.37	0.32	19.59
31	Type 1	2.67	30.33	0.24	5.86	0.45	18.55
30	Type 1	1.67	28.25	0.3	5.36	0.56	17.06
40	Type 1	2. 11	36.2	0.49	7.99	0.92	15.42
Au-Cu							
27	Type 2	8.38	22.63	4.45	0.29	0.02	8.63
Au-Ag-Pb							
21	Type 3	6.98	41.02	0.91	2.07	0.27	7.7
24	Type 3	7.13	32.13	0.3	1.42	0.4	4.74
25	Type 3	6.33	31.16	0.31	0.83	0.28	4.33
26	Type 3	6.31	38.07	0.67	0.48	0.38	6.42
28	Type 3	4.66	21.17	0.49	0.57	0.06	4.88

massive sulphide lenses confirm that they formed during separate volcanic episodes (Caté et al., 2014b, 2015). Discordant stockwork mineralization is spatially associated with the upper lenses (10 and 11) but has not been recognized in association with the lower lenses. Substantial Au enrichment is most closely associated with discordant Cu-Au stockwork mineralization in the 27 Lens and with broadly conformable disseminated Au-Ag-Pb-Cu mineralization in the 21, 24, 25, 26, and 28 lenses. The largest zone of Au-Ag-Pb-Cu mineralization is in the footwall of the 20 massive sulphide lens and is underlain by the discordant Cu-Au stockwork mineralization of the 27 Lens. Brief descriptions of the main massive sulphide ore lenses and their different host rocks are given below.

10 and 11 Lenses

The 10 and 11 lenses are structurally and stratigraphically the highest ore zones in the Lalor volcanic sequence. The 10 Lens consists of massive and semi-massive pyrite and sphalerite within quartz-muscovite-pyrite schist (K-alteration association). Chloritic zones with stringer chalcopyrite mineralization occur at the base of the 10 Lens. In most places, the contact between the hanging-wall rocks and the massive sulphides is sharp; locally there is a narrow transition from semi-massive pyrite-sphalerite into quartz-muscovite-pyrite schist. Wall rocks immediately above the 10 and 11 lenses are strongly pyritized, with abundant muscovite and kyanite. Locally, kyanite comprises up to 25 vol.% of the rock as porphyroblasts up to 2 cm in size.

The contact between the massive sulphides and the underlying chloritic schist is generally gradational, with increasing chlorite and chalcopyrite content and decreasing pyrite and sphalerite in the footwall. Massive chlorite is common in the ore zones. Volcanic rocks in the footwall contain abundant quartz, biotite, and chlorite, with coarse Mg-Fe amphibole (anthophyllite), kyanite, staurolite, and garnet porphyroblasts (K-Mg-Fe and Mg-Fe alteration association). Garnet is most commonly almandine garnet, which can vary from centimetre-sized up to massive 10 cm porphyroblasts. Although Cu-rich stockwork mineralization is well developed beneath the 10 Lens, the 11 Lens lacks a stringer zone and is thought to be a structurally dislocated portion of the 10 Lens.

20 Lens

The 20 Lens also consists of massive and semi-massive pyrite and sphalerite, but the hydrothermal alteration zoning in the immediate host rocks is more complex, owing to the presence of several different parent lithologies. In section 5300 N, the hanging wall is a quartz-biotite-muscovite-kyanite assemblage (K-alteration association), similar to the hanging wall of the 10 and 11 lenses and weakly altered intermediate rocks. Further north (section 5600 N), the hanging wall is chlorite schist with abundant carbonate that is locally associated with Ca-rich (skarn-like) diopside, epidote, grossular, and actinolite-tremolite alteration. Bright orange Ca-rich grossular is locally present in this alteration style. The footwall is dominantly chlorite-carbonate schist, but kyanite, muscovite, garnet, staurolite, anthophyllite, and/or talc are also present, representing complex transitions between the K, K-Mg-Fe, Mg-Fe, Mg-Ca, and Ca associations.

30, 31, and 40 Lenses

The 30, 31, and 40 lenses consist of both massive and semi-massive sulphides, with carbonate, actinolite and chlorite gangue minerals. The hanging wall and footwall of the 30 and 31 lenses consist of alternating chlorite-carbonate and chlorite-actinolite/tremolite assemblages (Ca-Mg-alteration association: Caté et al., 2015). Coarse magnetite crystals are also present in the hanging wall. The 40 Lens is the deepest zone of massive sulphides in the mine but it is thought to have formed at the same stratigraphic horizon as the 30 and 31 lenses, owing to the presence of similar host rocks and alteration styles. Quartz, plagioclase, and biotite, with abundant garnet and minor anthophyllite, are dominant about 15 m below the ore zone and are considered to represent the metamorphic equivalent of moderately altered mafic, intermediate, and felsic volcanic rocks in the footwall of the lenses (Caté et al., 2014).

METAL ZONATION

The 10 Lens shows the expected VMS zonation, with

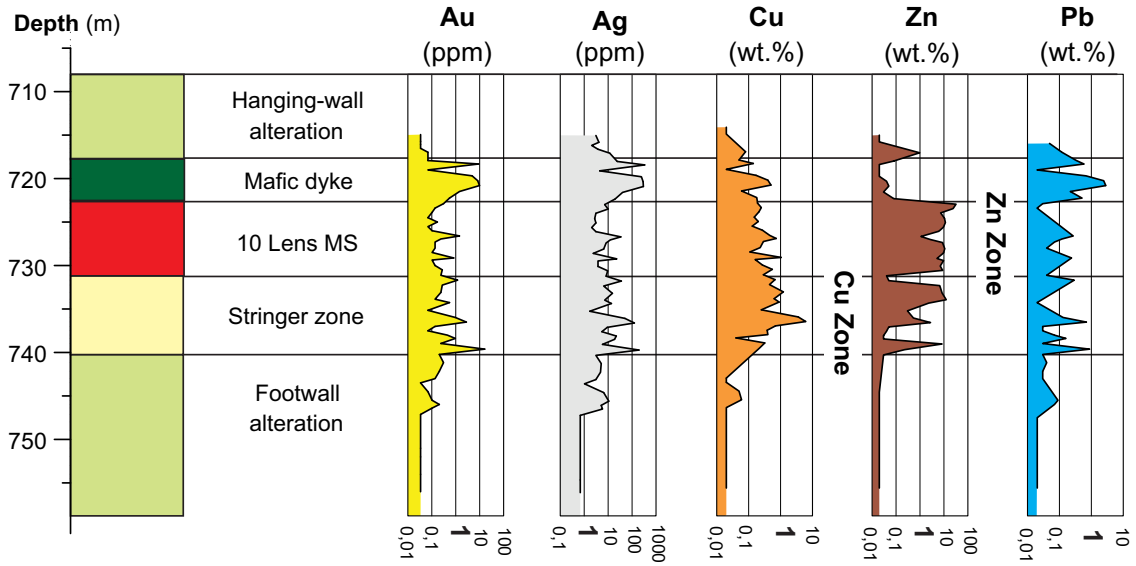

Figure 4. Composite graphic log of metal zonation in drillholes DUB174 and DUB239 through the 10 Lens massive sulphide zone, showing the expected volcanogenic massive sulphide zonation with Fe-Zn in the upper portion of the lens and then Cu-Au stringer mineralization at the base.

Fe-Zn in the upper portion of the lens and a discordant, although strongly transposed, Cu-Au stringer zone at the base (Fig. 4). The 20 Lens lacks a Cu-Au stringer zone but is underlain (and possibly partly overprinted) by disseminated Au-Ag-Pb-Cu-rich mineralization. A large portion of the Au-rich 21 Lens cuts the western part of the 20 Lens (on section 5600 N) and extends into the hanging wall. The 31 Lens is similarly cut by the Au-rich 25 Lens. For the most part, however, the Au-Ag-Pb-Cu-rich ore zones are broadly conformable. This conformable nature may indicate that heterogeneous permeability of the volcanic pile was a major control on mineralization. The large zone of semi-massive and stockwork-like chalcopyrite mineralization in the 27 Lens is stratigraphically the lowest occurrence of ore in the mine and may have been a central feeder zone for the entire deposit, in agreement with the high-temperature alteration in this part of the sequence (Caté et al., 2014; Mercier-Langevin et al., 2014). Although metamorphic remobilization of metals is apparent in all ore types, the scale of the remobilization is generally restricted to the ore lenses, with the large-scale metal zonation remaining intact (see also Gagné et al., 2007).

ORE TYPES OF THE LALOR DEPOSIT

Four main ore types have been identified among the different ore lenses (Table 3). Some can be compared to mineralization typical of unmetamorphosed VMS deposits, but others may be hybrid ore types related to hydrothermal overprinting and the effects of metamorphic recrystallization and remobilization.

Type 1 Fe-Zn Massive Sulphide

Fe-Zn-rich massive sulphide (Fig. 5a,b) is volumetrically the most abundant ore type and dominates in 6 of the 12 delineated ore lenses. The 10 and 11 Fe-Zn lenses are contained mostly within quartz-muscovite-pyrite rocks of the K-alteration association, and the 20, 30, 31, and 40 Fe-Zn lenses are mostly hosted by chlorite-carbonate-actinolite/tremolite schists of the Mg-Ca-alteration association (Caté et al., 2015). Disseminated pyrite is abundant in the quartz-muscovite-altered rocks (Fig. 5c). Although mostly intact bodies, slivers of the ore lenses, up to several metres across, occur in the adjacent wall rocks, displaced from the lenses by folding and transposition. Similarly, large enclaves of altered and foliated wall rocks are locally enclosed within massive sulphides (e.g. Bailes, 2011;

Figure 5 (opposite page). Photographs of representative ore types in NQ drill core (47.6 mm or 1-7/8 in diameter) from the Lalor deposit. **a)** Type 1 Fe-Zn-rich massive sulphide from 10 Lens (drillhole DUB174, 834.3–838.6 m), containing mostly euhedral pyrite with atoll structures in a matrix of Fe-rich sphalerite. **b)** Type 1 massive pyrite-sphalerite ore from 10 Lens (drillhole DUB205, 788.0–805.0 m). **c)** Disseminated pyrite in the foliations of a quartz-biotite schist from the hanging wall of the 31 Lens (drillhole DUB174, 872.0 m). **d)** Type 2 semi-massive chalcopyrite with pyrrhotite from the type locality in the 27 Lens (drillhole DUB263W05, 1270 m). **e)** Type 2 stockwork chalcopyrite mineralization with garnet porphyroblasts in a quartz-biotite matrix (Mg-Fe alteration association) from the 27 Lens (drillhole DUB263W05). **f)** Type 2 massive chalcopyrite with large garnet porphyroblasts from the 27 Lens (drillhole DUB262W05, 1271.3 m). **g)** Type 3 Au-Ag-Pb-Cu galena-sulphosalts-chalcopyrite ore in chlorite-carbonate-actinolite schist (Mg-Ca alteration association), typical of the 21, 24, and 25 lenses (drillhole DUB210, 1038.8 m). The fine-grained, steel grey matrix is galena. **h)** Type 4 low-sulphide ore with disseminated chalcopyrite-pyrrhotite-pyrite in quartz-chlorite-biotite schist (Mg-Fe alteration association) from the 25 Lens (drillhole DUB245; 995.8–1005.9 m).

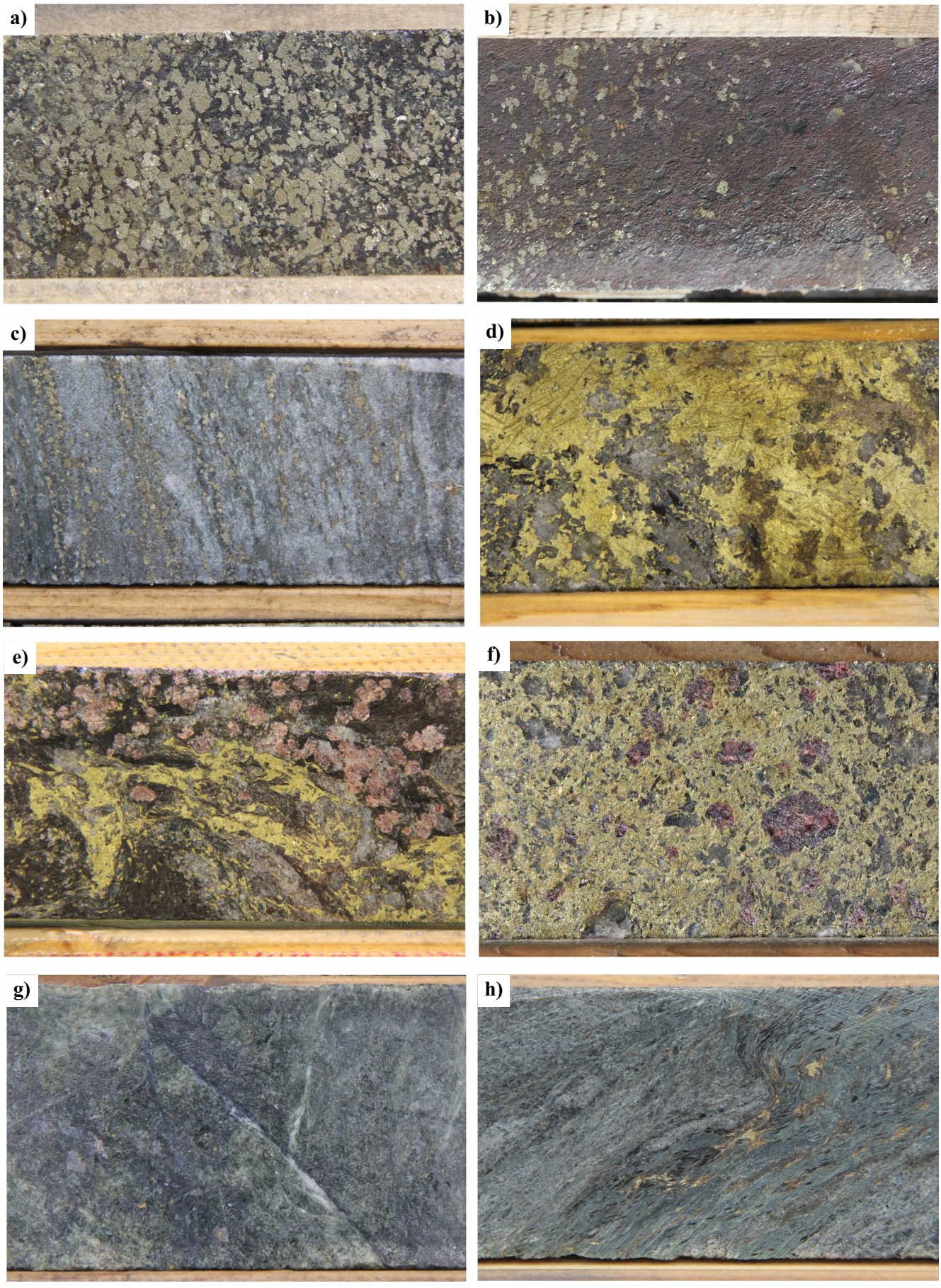
a)
b)
c)
d)
e)
f)
g)
h)

Table 3. Principal ore types of the Lalor volcanogenic massive sulphide deposit, Snow Lake.

Ore Type		Dominant Sulphides	Host Rock and Gangue Minerals
Type 1 (Fe-Zn)	Massive sulphides	Coarse-grained pyrite, sphalerite, ±pyrrhotite, ±chalcopyrite, ±galena	Quartz-muscovite schist
Type 2 (Au-Cu)	Semi-massive and stockwork	Semimassive and stringer chalcopyrite, ±pyrrhotite	Garnetiferous quartz-biotite schist and gneiss; large garnet porphyroblasts, ±cordietite, ±anthophyllite, ±staurolite
Type 3 (Au-Ag-Pb)	Chlorite-carbonate	Stringer and disseminated galena, ±sulphosalts, ±pyrite, ±sphalerite, ±chalcopyrite, ±pyrrhotite	Chlorite-carbonate schist; mainly dolomite and calc-silicates (epidote, grossular, diopside)
Type 4 (±Au)	Low-sulphide	Disseminated and stringer pyrite, ±chalcopyrite, ±pyrrhotite, ±sphalerite	Quartz-biotite-chlorite schist; ±almandine garnet, ±anthophyllite, ±staurolite

Caté et al., 2014a). The sulphide mineralogy is generally the same in all of the lenses and is dominated by pyrite and sphalerite (10–70 vol.%); pyrrhotite and chalcopyrite are minor minerals (less than 10 vol.%). Galena is rare but present in fractures and tension gashes within fold hinges and especially where several mafic intrusions cut the upper massive sulphide lenses (10 and 11). The mafic dykes are folded, boudinaged, and S_2-foliated, suggesting that they were intruded before the main D_2 deformation, and remobilized sulphides are common at their margins and in crosscutting fractures. A number of features clearly indicate the extent of recrystallization and annealing of the massive sulphides, including the presence of coarse-grained polycrystalline aggregates with well developed triple junctions, large pyrite porphyroblasts (up to 5 cm), and *durchbewegung* texture (see below).

Type 2 Cu-Au-Rich Semi-Massive and Stockwork Mineralization

The Cu- and Au-rich semi-massive and stockwork mineralization is hosted in garnetiferous chlorite schist of the Mg-Fe alteration association immediately beneath the 10 Lens, and at depth in intensely altered quartz- and biotite-bearing rocks. Semi-massive (10–60 vol.%) chalcopyrite occurs in the immediate stratigraphic footwall of the 10 Lens, and disseminated and stringer mineralization (<10 vol.% chalcopyrite) grades outward into the surrounding wall rock. Masses of pyrrhotite are present locally within the chalcopyrite (Fig. 5d). In contrast, the strongly transposed, stockwork-like Cu-Au mineralization in the 27 Lens, much deeper in the footwall, is not physically connected to massive sulphide ore higher up in the Lalor volcanic succession. The semi-massive chalcopyrite-pyrrhotite ore typically contains abundant quartz and biotite, and large (0.5–5 cm) garnet porphyroblasts that are commonly surrounded by networks of remobilized chalcopyrite (Fig. 5e,f). Quartz flooding and veins of quartz with ankerite are also common. The adjacent wall rocks, which consist of the deep footwall, transposed high-temperature Mg-Fe alteration association (Mercier-Langevin et al., 2014; Caté et al., 2015), commonly contain quartz, cordierite, and anthophyllite with minor chlorite, and locally porphyroblasts of staurolite and garnet. The anthophyllite forms arborescent growths up to 5 cm in length, and the cordierite occurs as royal blue massive aggregates.

Type 3 Au-Ag-Pb-Cu-Rich Ore

The main precious metal-rich ore consists mostly of disseminated sulphides and sulphosalts comprising up to 5 vol.% galena (Fig. 5g) and 2 vol.% chalcopyrite. The nature of the host rock varies but garnet- and amphibole-bearing rocks of the Mg-Fe chemical alteration association and chlorite-actinolite and Fe-dolomite-calcite schist of the Mg-Ca and Ca association (e.g. footwall of the 20 Lens) are the most common host. Pyrite, sphalerite, chalcopyrite, and pyrrhotite are minor components that commonly occur as isolated grains in the cleavages of chlorite and in low-pressure zones between porphyroblasts of garnet.

Figure 6 (opposite page). Photomicrographs of representative ore textures in the main ore types of the Lalor deposit. **a)** Type 1 Fe-Zn massive sulphide with a large, fractured poikiloblastic pyrite grain infilled by pyrrhotite and chalcopyrite, in a matrix of dark grey sphalerite (drillhole DUB195, 824.3 m, reflected plane polarized light (PPL), field of view (FOV)=4.4 mm). **b)** Type 1 Fe-Zn massive sulphide with large poikiloblastic pyrite euehdra in a matrix of massive sphalerite (drillhole DUB195, 823.2 m, transmitted light, FOV=4.4 mm). **c)** Disseminated pyrite, chalcopyrite, and arsenopyrite rimming quartz inclusions in massive sphalerite. A gold grain is adjacent to chalcopyrite at the rim of a rounded quartz inclusion (drillhole DUB210, 1045.0 m, reflected PPL, FOV=1 mm). **d)** Close-up of Type 2 semi-massive Cu-Au ore in drill core showing chalcopyrite occurring as rims on, and inclusions in, large (1 cm) garnet porphyroblasts (drillhole DUB262W05, 1271.3 m). **e)** Typical poikiloblastic garnet with inclusions of pyrite, pyrrhotite, and chalcopyrite (drillhole DUB262W01, 980.5 m, reflected PPL, FOV=1 mm). **f)** Typical fine-grained disseminated galena in quartz (drillhole DUB210, 1045.0 m, reflected PPL, FOV=1.1 cm). **g)** Pyrite and pyrrhotite in cleavages within quartz-chlorite-biotite hosting Type 2 Cu-Au ore (drillhole DUB258W01, 946.5 m, reflected PPL, FOV=4.4 mm). h) Typical texture of sulphides in cleavages within quartz-muscovite-garnet schist (drillhole DUB205, 815.2 m, transmitted light, FOV=4.4 mm).

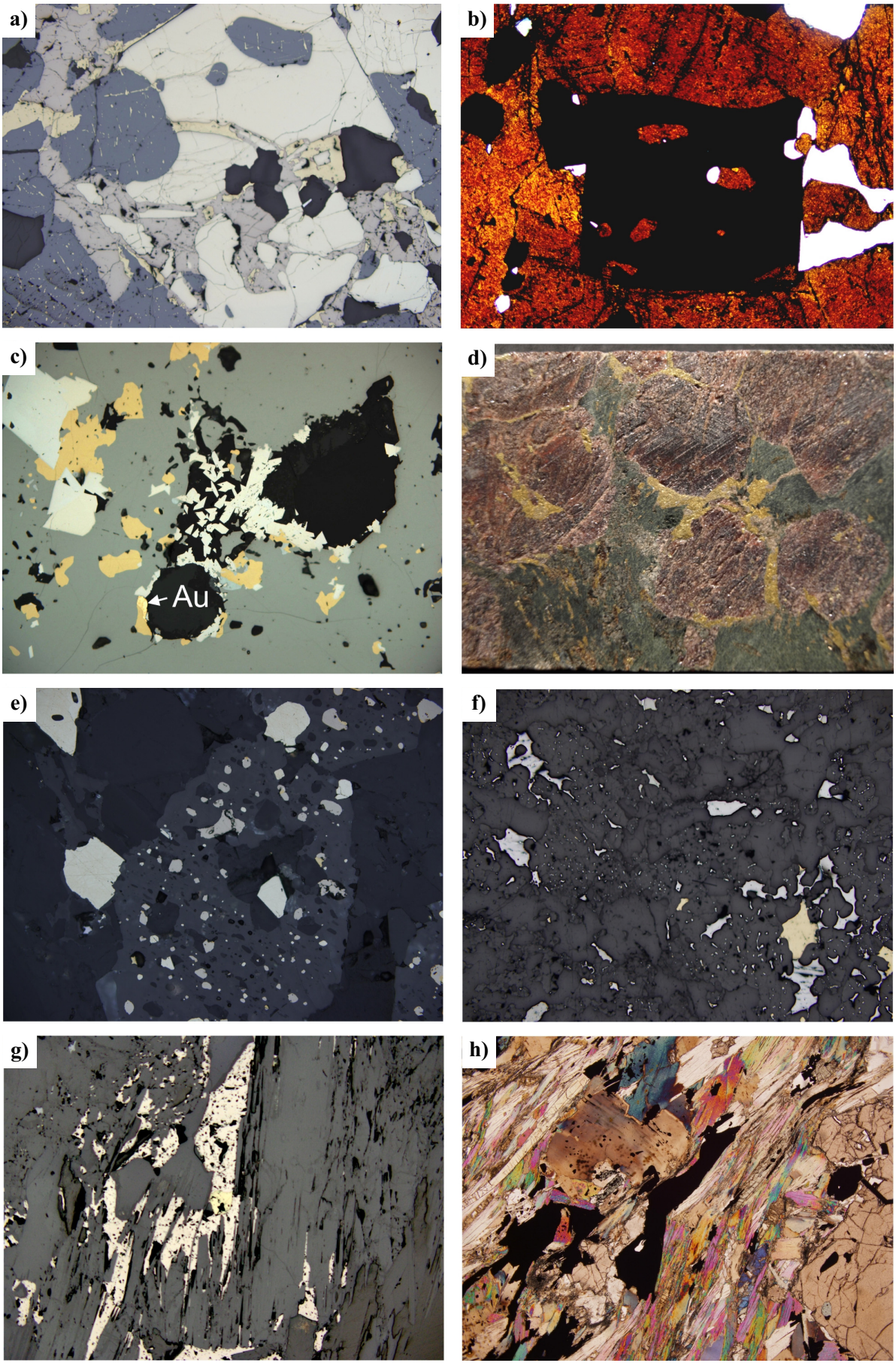
a)
b)
c)
Au
d)
e)
f)
g)
h)

This style of mineralization is typically isolated from the main massive sulphide lenses and is best developed in the 21, 24, 25 West, 26 and 28 lenses. In general, the galena is a strong prognostic indicator of Au grade in all of these lenses. The chlorite-carbonate-actinolite rocks locally include skarn-like assemblages with a variety of calc-silicates (epidote, grossular, diopside ± scapolite), corresponding to the Mg-Ca and Ca alteration associations of Caté et al. (2015).

Type 4 Low-Sulphide Quartz-Pyrite Mineralization

Low-sulphide quartz-pyrite ore consists of quartz-biotite-anthophyllite rock with a distinctive gneissic or schistose texture. This ore type has locally high Au grades. Sulphide contents do not exceed 10 vol.% and generally do not correlate with Au grade. Pyrite is dominant, but chalcopyrite, sphalerite, and pyrrhotite are present locally in low-pressure zones between cleavages of the major phyllosilicate minerals and adjacent to porphyroblasts (Fig. 5h). Staurolite and anthophyllite are also present locally. Type 4 mineralization is spatially associated with Au-Ag-Pb-Cu-rich galena-sulphosalts-chalcopyrite ore in several lenses (e.g. in the 21, 24, and 25 lenses) and occurs in the same broad zones of mineralization and locally grades into Au-Ag-Pb-Cu-rich ore over distances of a few metres.

ORE MINERALOGY AND MINERAL CHEMISTRY

Pyrite

In the massive sulphide lenses, pyrite occurs as coarse-grained polycrystalline aggregates, in 2–5 cm patches with intergranular sphalerite. Elsewhere, pyrite occurs as isolated porphyroblasts in a homogenous sphalerite matrix. In many places, pyrite porphyroblasts show evidence of brittle deformation with fractures filled by sphalerite and other sulphides (Fig. 6a,b). In other places, pyrite and sphalerite are clearly segregated into discontinuous gneissic bands. Classic durchbewegung texture is common, in which hard (6.0–6.5), brittle pyrite and locally quartz nodules show evidence of rotation in a flowing matrix of softer (ductile) sphalerite (Fig. 7; Craig and Simpson, 1991). All analyzed pyrite is nearly stoichiometric FeS_2. However, some pyrite contains up to 2 wt% Co, especially where intergrown with pyrrhotite. Some pyrite also contains up to 0.1 wt% Ni and up to 1 wt% As (Table 4).

Sphalerite

Sphalerite in the massive sulphide lenses is coarsely crystalline "blackjack", with high Fe contents (Table 4). Where it is most abundant, sphalerite is commonly associated with Fe-rich carbonate. Coarse-grained polycrystalline aggregates with curved or straight grain boundaries are most common, but locally the sphalerite occurs in homogenous masses, typically with chalcopyrite inclusions distributed in a gridded network (e.g. chalcopyrite disease: Barton and Bethke, 1987) (Fig. 6a) or more commonly remobilized to grain boundaries (Fig. 6c). The average Fe content of sphalerite is 7.65 wt% (more than 15 mol.% FeS: Table 4) and is very homogeneous throughout most of the deposit. Cd contents are generally low (<5 wt%, average 2.3 wt%). Hg is present in detectable abundances but never exceeds 0.10 wt%. In the 40 Lens, the sphalerite is orange, indicating much lower Fe contents, which contrasts with the blackjack sphalerite in the rest of the deposit and may possibly be a result of metamorphic reactions.

Figure 7. Photograph of classic *durchbewegung* texture (Craig and Simpson, 1991) in type 1 Fe-Zn-rich massive sulphide ore (DUB195, 809.7 m). The texture shows rounded nodules of hard pyrite and quartz nodules in a matrix of softer sphalerite. NQ drill core (47.6 mm or 1-7/8 in diameter).

Chalcopyrite, Bornite, and Cubanite

Disseminated chalcopyrite is present as isolated blebs and anhedral masses in the massive sulphide ores, and these generally increase in abundance toward the bottoms of the lenses. In the Cu-Au stockwork zones, chalcopyrite occurs as discrete stringers within the main foliation of the altered host rocks, rimming large garnet porphyroblasts (Fig. 6d), and disseminated in the cleavages of the major gangue minerals. The chalcopyrite is nearly stoichiometric $CuFeS_2$ throughout the deposit (Table 4), although several grains of Ag-bearing chalcopyrite (up to 4 wt% Ag) were identified in association with Ag-sulphosalts. Traces of cubanite are present as exsolution lamellae in the chalcopyrite, typically as thin peach-coloured flames and locally as distinct crystallographically controlled bands intersecting at 60 and 120°. Bornite also occurs locally as inclusions in chalcopyrite and rarely with galena, electrum, and sulphosalts in Type 3 Au-Ag-Pb-Cu-rich ore.

Pyrrhotite

Pyrrhotite is present in the massive sulphide ores, com-

Table 4. Electron microprobe analyses of selected ore minerals of the Lalor massive sulphide deposit (average, minimum, and maximum values for n samples).

Mineral	(n)	S	Fe	Co	Ni	Cu	Zn	Ga	As	Se	Ag	Cd	In	Sn	Sb	Te	Au	Hg	Pb	Bi	Total
Major and Minor Minerals																					
Pyrite	27	53.7	47.29	0.27	0.02	0.01	0.02	0.01	0.11	0.02	0.02	0.02	0.01	0.01	<0.01	0.01	0.03	0.03	<0.01	0.12	101.71
FeS_2	min	52.23	45.61	<0.01	<0.01	<0.01	<0.01	<0.01	<0.01	<0.01	<0.01	<0.01	<0.01	<0.01	<0.01	<0.01	<0.01	<0.01	<0.01	<0.01	100.54
	max	55.18	48.07	2.08	0.12	0.09	0.09	0.07	1.4	0.05	0.09	0.07	0.04	0.05	<0.01	0.08	0.1	0.14	0.09	0.21	103.5
Pyrrhotite	30	38.8	60.97	0.01	0.02	0.02	0.02	0.02	0.01	0.02	0.02	0.01	<0.01	0.01	<0.01	0.01	0.03	0.01	0.06	0.09	100.13
FeS	min	37.39	59.9	<0.01	<0.01	<0.01	<0.01	<0.01	<0.01	<0.01	<0.01	<0.01	<0.01	<0.01	<0.01	<0.01	<0.01	<0.01	<0.01	<0.01	98.94
	max	40	62	0.05	0.13	0.14	0.09	0.09	0.05	0.09	0.11	0.07	0.05	0.05	<0.01	0.04	0.14	0.09	0.47	0.23	101.54
Sphalerite	19	32.24	7.65	0.01	0.01	0.54	55.97	0.18	0.01	0.02	0.01	2.32	<0.01	0.01	0.01	<0.01	0.04	0.02	0.05	0.07	99.17
ZnS	min	31.56	3.85	<0.01	<0.01	<0.01	52	0.04	<0.01	<0.01	<0.01	0.02	<0.01	<0.01	<0.01	<0.01	<0.01	<0.01	<0.01	<0.01	96.77
	max	32.82	9.24	0.03	0.07	3.57	60.14	0.32	0.03	0.06	0.06	5.1	0.05	0.06	0.07	0.01	0.16	0.09	0.35	0.17	100.94
Chalcopyrite	13	34.34	30.56	0.01	0.01	34.41	0.05	0.01	0.01	0.03	0.04	0.03	<0.01	0.01	0.01	0.01	0.02	0.01	0.09	0.07	99.72
$CuFeS_2$	min	33.91	29.84	<0.01	<0.01	34.04	<0.01	<0.01	<0.01	<0.01	<0.01	<0.01	<0.01	<0.01	<0.01	<0.01	<0.01	<0.01	<0.01	<0.01	98.21
	max	34.74	30.88	0.03	0.03	34.88	0.15	0.03	0.04	0.07	0.26	0.07	0.01	0.03	0.15	0.03	0.08	0.11	0.29	0.24	100.44
Cubanite	6	34.85	41.06	<0.01	0.02	23.3	<0.01	0.02	<0.01	0.02	0.09	0.01	0.01	0.01	<0.01	0.01	0.04	0.01	0.11	0.12	99.67
$CuFe_2S_3$	min	34.43	40.51	<0.01	<0.01	23.11	<0.01	<0.01	<0.01	<0.01	<0.01	<0.01	<0.01	<0.01	<0.01	<0.01	<0.01	<0.01	<0.01	0.07	98.4
	max	35.42	41.39	0.01	0.06	23.49	0.01	0.05	0.01	0.05	0.26	0.03	0.04	0.02	<0.01	0.04	0.23	0.04	0.38	0.2	100.51
Arsenopyrite	8	21.68	35.97	0.02	0.01	0.18	0.04	<0.01	42.63	0.27	0.02	0.01	<0.01	0.01	0.25	0.1	0.04	0.02	0.05	0.05	101.35
FeAsS	min	20.13	34.67	<0.01	<0.01	<0.01	0.01	<0.01	39.15	0.22	<0.01	<0.01	<0.01	<0.01	<0.01	0.01	<0.01	<0.01	<0.01	<0.01	98.97
	max	24.61	37.4	0.05	0.02	0.62	0.14	<0.01	45.47	0.31	0.06	0.07	0.03	0.04	1.73	0.23	0.11	0.11	0.19	0.14	101.98
Galena	12	13.59	0.03	0.01	<0.01	0.05	0.04	0.01	<0.01	0.38	0.05	0.04	<0.01	0.01	0.05	0.04	0.02	<0.01	85.3	0.06	99.71
PbS	min	13.19	<0.01	<0.01	<0.01	0.01	<0.01	<0.01	<0.01	0.05	<0.01	<0.01	<0.01	<0.01	<0.01	<0.01	<0.01	<0.01	84.49	<0.01	98.92
	max	13.92	0.18	0.03	0.01	0.18	0.1	0.04	0.03	0.6	0.22	0.13	0.03	0.04	0.15	0.12	0.09	0.04	86.03	0.3	100.66
Gold	7	0.06	0.79	0.01	0.01	0.09	<0.01	0.17	0.02	<0.01	22.99	0.01	<0.01	0.3	0.01	0.03	73.94	2.67	0.01	0.02	101.13
(Au,Ag)	min	<0.01	0.07	<0.01	<0.01	<0.01	<0.01	<0.01	<0.01	<0.01	12.1	<0.01	<0.01	<0.01	<0.01	<0.01	63.22	<0.01	<0.01	<0.01	100.26
	max	0.12	2.66	0.02	0.03	0.21	<0.01	0.61	0.07	0.01	29.19	0.08	<0.01	1.32	0.07	0.07	87.52	7.95	0.04	0.17	101.98
Electrum	11	0.05	0.17	0.01	0.01	0.11	0.02	<0.01	0.03	0.01	50.85	0.06	<0.01	0.13	0.62	0.09	43.83	3.88	0.05	0.01	99.92
(Au,Ag)	min	<0.01	<0.01	<0.01	<0.01	<0.01	<0.01	<0.01	<0.01	<0.01	40.21	<0.01	<0.01	<0.01	<0.01	0.06	16.86	0.09	<0.01	<0.01	98.21
	max	0.19	0.39	0.04	0.03	0.33	0.2	<0.01	0.28	0.02	78.55	0.3	<0.01	0.97	2.68	0.16	54.53	7.49	0.28	0.16	101.59
Tetrahedrite	7	25.53	6.38	<0.01	<0.01	37.77	0.76	<0.01	7.24	0.09	3.68	0.07	<0.01	0.06	19.17	<0.01	0.01	<0.01	0.01	0.05	100.85
$(Cu,Ag)_{12}(Sb,As)_4S_{13}$	min	24.38	6.01	<0.01	<0.01	34.19	0.32	<0.01	1.13	0.04	1.44	<0.01	<0.01	0.02	15.34	<0.01	<0.01	<0.01	<0.01	<0.01	99.62
	max	26.41	6.77	0.01	0.02	40.16	1.22	0.01	9.96	0.13	6.94	0.15	0.01	0.13	27.3	<0.01	0.05	0.01	0.08	0.15	101.78
Freibergite	13	22.6	5.73	0.01	0.01	23.04	0.67	<0.01	1.66	0.03	20.54	0.42	<0.01	0.07	24.86	<0.01	0.02	<0.01	0.07	0.04	99.77
$(Ag,Cu)_{12}(Sb,As)_4S_{13}$	min	18.58	5.05	<0.01	<0.01	12.85	0.25	<0.01	0.03	<0.01	12.39	0.12	<0.01	<0.01	14.26	<0.01	<0.01	<0.01	<0.01	<0.01	98.01
	max	24.99	7.22	0.04	0.04	30.34	1.16	<0.01	10.05	0.22	36.65	1.08	<0.01	0.12	28.18	<0.01	0.06	<0.01	0.35	0.15	101.22

Table 4 continued.

Mineral	(n)	S	Fe	Co	Ni	Cu	Zn	Ga	As	Se	Ag	Cd	In	Sn	Sb	Te	Au	Hg	Pb	Bi	Total
Bournonite (As)	9	19.85	0.05	0.01	0.01	13.03	0.03	0.01	1.76	0.27	0.02	0.03	0.01	0.11	22.66	0.04	<0.01	<0.01	41.94	0.09	99.92
$PbCuSbS_3$	min	19.31	<0.01	<0.01	<0.01	12.52	<0.01	<0.01	0.09	0.11	<0.01	<0.01	<0.01	0.07	18.22	<0.01	<0.01	<0.01	41.29	<0.01	99.07
	max	20.32	0.2	0.03	0.05	13.61	0.1	0.05	4.78	0.43	0.07	0.1	0.03	0.14	25.13	0.14	0.01	<0.01	42.43	0.17	101.07
Boulangerite (As)	4	18.3	0.04	0.01	<0.01	0.05	0.02	<0.01	0.47	0.17	0.18	0.07	<0.01	0.12	25.13	<0.01	0.03	<0.01	54.23	0.09	98.92
$Pb_5Sb_4S_{11}$	min	18.2	<0.01	<0.01	<0.01	<0.01	<0.01	<0.01	0.02	<0.01	<0.01	<0.01	<0.01	0.09	24.27	<0.01	<0.01	<0.01	53.6	<0.01	98.32
	max	18.45	0.14	0.01	<0.01	0.2	0.06	<0.01	1.74	0.32	0.69	0.18	<0.01	0.15	26	<0.01	0.11	<0.01	54.85	0.27	99.18
Allargentum	4	2	0.02	0.01	<0.01	0.08	<0.01	<0.01	0.05	0.01	75.02	0.3	<0.01	0.01	17.99	0.05	4.65	0.13	0.07	0.02	100.4
$Ag_{1-x}Sb_x$	min	0.88	<0.01	<0.01	<0.01	<0.01	<0.01	<0.01	<0.01	<0.01	73.24	0.25	<0.01	<0.01	13.91	<0.01	1.76	<0.01	<0.01	<0.01	99.11
	max	3.19	0.04	0.02	<0.01	0.2	<0.01	<0.01	0.08	0.02	77.17	0.34	<0.01	0.03	20.11	0.1	7.35	0.35	0.14	0.05	102.1
Trace Minerals																					
Ag-Chalcopyrite $CuFeS_2$	2	32.45	28.96	<0.01	<0.01	32.19	0.03	0.05	0.03	0.03	3.71	0.02	<0.01	<0.01	<0.01	0.01	0.04	<0.01	0.19	0.05	97.75
Galena (Se) Pb(S,Se)	3	12.51	0.53	0.02	<0.01	0.01	0.04	0.01	<0.01	2.45	0.06	0.02	<0.01	0.09	0.03	0.04	0.04	<0.01	83.89	<0.01	99.75
Cobaltite CoAsS	1	19.96	4.97	29.46	0.46	<0.01	<0.01	<0.01	43.32	0.3	<0.01	<0.01	<0.01	0.05	1.07	<0.01	0.04	<0.01	0.1	0.14	99.86
Gudmundite FeSbS	2	15.14	26.78	<0.01	0.16	0.05	<0.01	0.05	0.27	0.01	0.01	<0.01	<0.01	0.25	58.5	0.09	0.03	<0.01	0.08	0.01	101.42
Meneghinite $Pb_{13}CuSb_7S_{24}$	2	17.86	<0.01	0.01	0.01	1.29	0.03	<0.01	0.06	0.18	0.05	<0.01	<0.01	0.06	19.77	0.01	0.02	<0.01	61.35	0.07	100.77
Sterryite $Ag_2Pb_{10}(Sb,As)_{12}S_{29}$	2	18.94	0.08	0.01	<0.01	0.36	0.07	0.02	0.11	0.19	3.62	<0.01	<0.01	0.15	26.86	<0.01	0.07	<0.01	49.69	0.02	100.19
Ag-Pentlandite $(Ag,Fe,Ni)_9S_8$	1	31.88	38.15	0.08	15.72	1.7	<0.01	<0.01	0.04	0.03	12.64	<0.01	<0.01	<0.01	<0.01	0.03	<0.01	<0.01	<0.01	0.05	100.31
Benleonardite $Ag_8(Sb,As)Te_2S_3$	1	6.07	0.04	<0.01	0.01	<0.01	<0.01	<0.01	0.01	0.39	63.3	0.23	<0.01	0.05	7.38	23.6	0.01	<0.01	<0.01	0.1	101.2
Stützite(?) Ag_5Te_3	1	1.23	1.8	<0.01	<0.01	0.15	0.03	<0.01	<0.01	0.02	57.83	0.28	<0.01	0.68	<0.01	31.76	0.06	0.1	1.31	<0.01	95.25

monly as rims around pyrite or in pressure shadows. It is always closely associated with chalcopyrite, especially in the Type 2 semi-massive and stockwork chalcopyrite ore. Locally pyrrhotite is also present in late quartz veins, commonly with gahnite. Like pyrite, the pyrrhotite is essentially stoichiometric FeS (Table 4). One euhedral grain of Ag-pentlandite $(Ag,Fe,Ni)_9S_8$ was identified intergrown with pyrrhotite and cubanite.

Galena

Galena is most abundant in Type 3 Au-Ag-Pb-Cu-rich ore. It is a minor (<5 vol.%) component of the massive sulphide ores where it occurs as coarse-grained aggregates in the 10 and 11 lenses and as finer grained disseminations in the lower lenses (30, 31, 40). It occurs most commonly as anhedral to subhedral masses at grain boundaries of pyrite and sphalerite (Fig. 6f). However, (remobilized) galena also occurs as coarse cubes up to 1 cm in size in some late quartz veins. In the Au-Ag-Pb-Cu ore, fine-grained galena occurs within the mineral cleavages of the host chlorite-carbonate-actinolite schist, where it is commonly associated with microscopic grains of electrum and sulphosalts. Galena is rare in the low-sulphide Au-rich zones (Type 4), but where present shows the same general paragenesis with electrum and sulphosalts. Galena contains up to 4 wt% Se but is generally Ag-poor (<0.2 wt%) and Te-poor (<0.1 wt%) (Table 4).

Pb-Sb-Sulphosalts

Numerous complex sulphosalts have been identified in the Type 3 Au-Ag-Pb-rich ore, together with galena, chalcopyrite, and electrum. These include tetrahedrite $[(Cu,Fe)_{12}Sb_4S_{13}]$, bournonite $[PbCuSbS_3]$, boulangerite $[Pb_5Sb_4S_{11}]$, and meneghinite $[Pb_{13}CuSb_7S_{24}]$. These minerals typically occur as fine-grained, complex intergrowths with galena and, less commonly, with chalcopyrite, freibergite (see below), and gold (Fig. 6c). The sulphosalts contain minor As (up to 4 wt%) , Se (up to 0.4 wt%), and Sn (up to 0.2 wt%) (Table 4).

Ag-Sulphosalts

The major Ag minerals, other than electrum, are Ag-bearing tetrahedrite, freibergite $[(Ag,Cu,Fe)_{12}(Sb,As)_4S_{13}]$, allargentum $[Ag_{1-x}Sb_x]$, and sterryite $[Ag_2Pb_{10}(Sb,As)_{12}S_{29}]$. They occur mainly as Ag-rich inclusions in galena and less commonly as intergrowths with chalcopyrite. Silver-bearing tetrahedrite (Table 4) contains 1 to 7 wt% Ag, freibergite contains up to 37 wt% Ag, and some grains are notably tarnished. Lam et al. (2014) also identified aurostibite $(AuSb_2)$, but this mineral was not found in the present study.

Ag-Bearing Telluride Minerals

Two Ag-bearing telluride minerals were identified by microprobe (Table 4). They are a Te-rich Ag-sulphide, possibly benleonardite $[Ag_8(Sb,As)Te_2S_3]$, intergrown with electrum, and a hessite-like mineral, possibly stutzite $[Ag_{5-x}Te_3]$, intergrown with chalcopyrite and sphalerite. Lam et al. (2014) also identified hessite $[Ag_2Te]$ and altaite [PbTe], but we did not encounter these minerals.

Gold and Electrum

The main Au-bearing mineral in Type 2 Au-Cu mineralization and Type 3 Au-Ag-Pb-rich ore is electrum. Electrum commonly occurs at the grain boundaries and in microfractures of larger grains of galena, commonly together with various Sb- and Ag-bearing sulphosalts, as inclusions in pyrite or chalcopyrite, and rimming quartz inclusions in the sulphides. The size of the electrum grain is up to 0.1 mm, but much smaller grains are common. Both gold (<30 wt% Ag) and electrum (40–80 wt% Ag) compositions were obtained, but the Au:Ag ratio is variable and averages approximately 2:1 (Table 4). Significant Hg (average 3.41 wt%) and traces of Sb (0.38 wt%) are also present. Both gold and electrum are Hg-rich, although gold contains only 2.5 wt% Hg (average of 7 analyses) and electrum commonly contains 6–7 wt% Hg. Gold was not detected by microprobe in any of the other ore minerals.

Other Trace Minerals

Arsenopyrite [FeAsS], cobaltite [CoAsS], and gudmundite [FeSbS] were found in a number of different ore types. Fine-grained, euhedral arsenopyrite is locally associated in the massive sulphides with tetrahedrite, galena, and electrum (Fig. 6c). Arsenopyrite contains up to 0.3 wt% Se but is otherwise free of trace elements (Table 4). Cobaltite and gudmundite occur together with pyrrhotite and chalcopyrite, and both contain up to 0.5 wt% Ni. Trace Bi occurs in some pyrite, pyrrhotite, and chalcopyrite grains (average 0.12 wt%; maximum 0.23 wt%), perhaps as micro-inclusions of Bi minerals.

ORE GEOCHEMISTRY

Table 5 lists the average bulk geochemical compositions of the different ore types determined for the 70 samples analyzed in this study. The samples of massive sulphide ore average 11.7 wt% Fe and 12.3 wt% Zn, corresponding to 25 wt% FeS_2 and 18 wt% ZnS. Zinc shows a strong correlation with Cd (r = 0.97), Hg (r = 0.61), In (r = 0.56), and Sb (r = 0.48). Fe shows a positive correlation with Co (r = 0.41) and Ni (r = 0.48), but not with Zn. The pyrite-rich ores and sphalerite-rich ores clearly represent geochemically distinct

Table 5. Average bulk compositions of selected ore types of the Lalor volcanogenic massive sulphide deposit.

Element	Unit	Massive Sulphide	Semi-Massive Chalcopyrite	Chlorite Carbonate	Low-Sulphide High-Au
		n = 26	n = 9	n = 26	n = 10
SiO_2	%	19.63	57.67	39.71	46.94
Al_2O_3		5.08	8.52	7.25	9.17
Fe_2O_3		13.25	2.08	2.9	4.32
FeO		15.1	13.4	8	14.1
MgO		3.3	7.48	9.94	8.23
MnO		0.2	0.12	0.25	0.29
CaO		3.05	1.81	10.52	1.45
Na_2O		0.16	0.07	0.08	0.11
K_2O		0.32	0.3	0.16	0.41
TiO_2		0.19	0.25	0.15	0.31
P_2O_5		0.06	0.16	0.06	0.16
CO_2		0.78	0.11	3.45	0.25
Total C		0.23	0.04	0.98	0.08
Total S		25.7	6.11	7.87	7.08
LOI		0.52	0.07	2.21	0.17
Cu		2.37	1.42	1.06	4.13
Zn		12.32	0.42	4.57	1.88
Pb		0.15	0.04	0.84	0.04
Au	ppm	10.5	44	147	11.4
Ag		51	124	365	66.4
As		356	102	38	57.5
Sb		93	2.2	8.6	2.4
Cd		307	17.1	107	49.2
Hg		83.12	1.01	14.84	5.53
Tl		0.21	0.2	0.74	0.15
Sn		14	3	9	16
In		0.6	0.2	0.2	0.4
W		26	2.4	1.1	4.4
Ga		10	11	12	14
Ge		1.6	0.8	1.2	1.1
Co		96	88	38	70
Ni		20	9	6	15
Se		122	74	121	77
Bi		1.2	0.4	5.8	2.8
Te		14	65.2	63.8	20.8
Mo		5	2	3	4
V		54	63	22	179
U		1.75	0.78	1.29	0.92
Th		1.1	1.67	1.41	2.1
Ba		37	37	31	78
Sr		30	12	38	16
Cs		0.1	0.2	0.1	0.2
F		250	860	510	600
B		1	2	1	<1
Be		<1	<1	<1	<1
Li		9	22	8	11
Hf		0.6	1	1.3	1.1
Ta		0.13	0.15	0.15	0.15
Zr		24	38	44	45
Nb		2.2	3.3	3.1	3.4
Sc		10	14	9	24
Y		5	10.5	16.7	11.5
∑REE		42.4	67.3	85.5	95.8

assemblages, despite their occurrence together in the massive sulphide lenses.

Copper, which is present mainly in the semi-massive chalcopyrite ore, shows a moderately strong correlation with Se (r = 0.48) and As (r = 0.63), and to a lesser extent with Sn (r = 0.39) and In (r = 0.27). Tin and In are common trace constituents of Cu-rich ores in other VMS deposits, typically in the chalcopyrite-like minerals stannite and roquesite, but these were not identified in the present study.

Gold shows the strongest correlation with Ag (r = 0.98) and Te (r = 0.80), but the precious metals are distributed bimodally, with equally high contents in the Pb-rich ores and Au-Cu ores, so the statistical correlations with Pb and Cu in the bulk ore are weak. Although galena is the most common visual prognostic indicator for precious-metal enrichment in the chlorite-carbonate-actinolite-altered zones, Pb has a very poor correlation with Au and Ag at the hand-specimen scale. The strong correlation of Ag with Au reflects the high Ag content of the electrum and the association of electrum with Ag-rich sulphosalts, especially in the precious metal-rich chlorite-carbonate-actinolite-altered zones. The correlation with Te suggests the presence of an unidentified Au-bearing telluride.

Principal components analysis confirms that the bulk geochemical compositions of the ores include a significant mafic volcanic component (TiO_2, Al_2O_3, Na_2O, P_2O_5, Sc, Th, Y, Cr, V), a felsic element component (Al_2O_3, Hf, Nb, Ta, Zr, and light rare earth elements), a phyllosilicate component (K_2O, Al_2O_3, Ba, Cs, Li, F, and Ga), a chloritic component (MgO, Al_2O_3, TiO_2, Mn), and a carbonate or calc-silicate component (CO_2, CaO, MgO, MnO, and Sr). CaO and CO_2 contents strongly correlate with Pb in the precious metal-rich Au-Ag-Pb-Cu-rich ores hosted in chlorite-carbonate-actinolite altered rocks, as well as with U, Th, Y, and heavy rare earth elements. The latter may reflect an association with secondary minerals (e.g. xenotime) that are the product of metamorphic remobilization. CaO is also weakly correlated with Sr, Mn, and MgO (present in dolomite but also in co-existing chlorite, actinolite, and tremolite).

SULPHUR AND LEAD ISOTOPES

Sulphur isotope compositions of pyrite, sphalerite, pyrrhotite, and chalcopyrite show a limited range from $\delta^{34}S$ 0.41 to 2.84 ‰ with no significant difference between minerals (Table 6). This narrow range is typical of sulphides that have been extensively recrystallized during metamorphism (e.g. Shanks 2001; Fig. 8). Although it has been shown that many sulphide minerals can retain their isotopic compositions through metamorphism (e.g. Corriveau and Spry, 2014), it is common for highly metamorphosed massive sulphide

Table 6. Sulphur isotope compositions of ore minerals from the Lalor massive sulphide deposit.

Sample	Lens	Ore Type	$\delta^{34}S$ (‰)	Mineral
517-Py	10	1	2.58	pyrite
518-Py	10	1	2.22	pyrite
521-Py	10	1	2.27	pyrite
545-Py	10	1	1.65	pyrite
632-Py	10	1	2.61	pyrite
635-Py	10	1	2.84	pyrite
637-Py	10	1	2.06	pyrite
643-Py	10	1	1.87	pyrite
651-Py	10	1	1.88	pyrite
666-Py	10	1	1.29	pyrite
545-Sp	10	1	0.93	sphalerite
667-Sp	10	1	0.41	sphalerite
664-Cp	10	1	1.36	chalcopyrite
516-Po	10	1	1.41	pyrrhotite
651-Po	10	1	1.83	pyrrhotite
664-Po	10	1	1.17	pyrrhotite
549-Cp	10	3	1.03	chalcopyrite
658-Py	10	3	0.85	pyrite
665-Cp	10	4	1.08	chalcopyrite
665-Po	10	4	1.22	pyrrhotite
536-Py	21	1	1.51	pyrite
595-Py	21	1	2.59	pyrite
596-Py	21	1	1.86	pyrite
536-Sp	21	1	1.72	sphalerite
559-Py	21	3	2.4	pyrite
611-Py	21	3	2.45	pyrite
559-Sp	21	3	1.6	sphalerite
598-Py	21/20	1	1.8	pyrite
599-Py	21/20	1	2.19	pyrite
598-Sp	21/20	1	1.36	sphalerite
618-Py	21/25	1	2.13	pyrite
608-Py	21/20	3	2.2	pyrite
619-Py	25	N/A	2.79	pyrite
562-Py	25	1	2.33	pyrite
587-Py	25	1-3	1.52	pyrite
524-Py	25	3	2.66	pyrite
586-Py	25	3	2.42	pyrite
575-Py	25/26	3	0.56	pyrite
538-Cp	27	2	2.34	chalcopyrite
539-Cp	27	2	1.84	chalcopyrite
540-Py	27	2	1.28	pyrite
578-Py	27	2	1.68	pyrite
538-Po	27	2	2.27	pyrrhotite
603-Cp	N/A	2	1.4	chalcopyrite
631-Py	N/A	2	1.96	pyrite
628-Cp	N/A	4	2.45	chalcopyrite
628-Py	N/A	4	2.3	pyrite
581-Py	Vein	N/A	0.96	pyrite
586-Sp	N/A	N/A	2.07	sphalerite

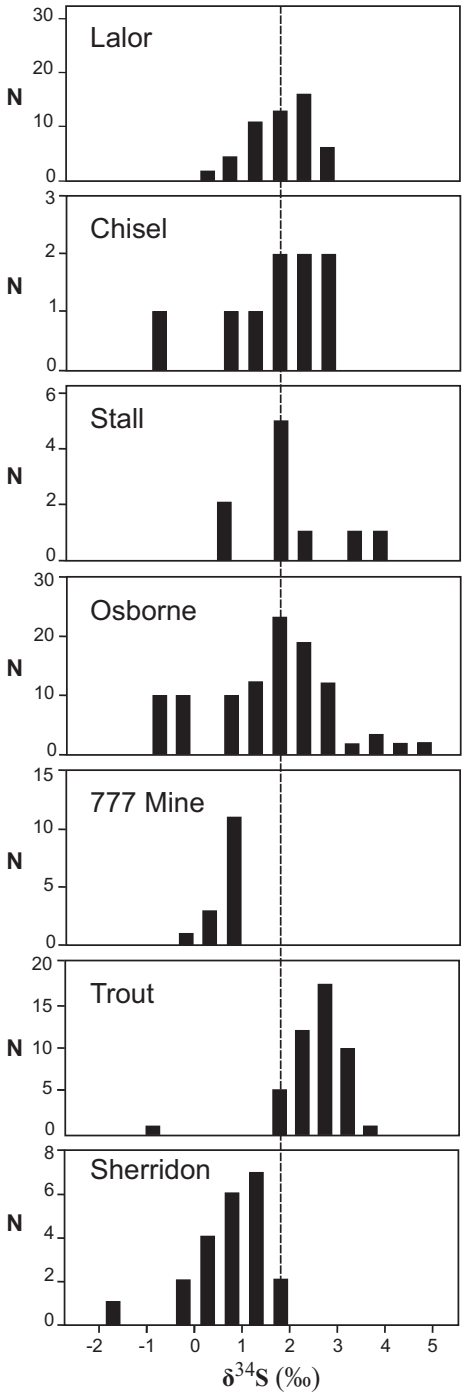

Figure 8. Histogram of sulphur isotope data from the Lalor massive sulphide deposit (Table 7), comparing the average value for Lalor sulphides (dashed line) with the distribution of $\delta^{34}S$ values for Chisel Lake and Stall in the Snow Lake camp (J.M. Franklin, unpublished data) and for the 777 Mine and Trout Lake Mine in Flin Flon (Polito et al., 2007). Data for the Sherridon sediment-hosted massive sulphide deposit are from (Sangster, 1972, 1978). Sulfide $\delta^{34}S$ values for Lalor range from 0.4 to 2.8 per mil (average +1.8 per mil), similar to all other Paleoproterozoic volcanogenic massive sulphide deposits in the region. Somewhat more variable compositions are evident at 777 and Trout Lake, at Osborne Lake northeast of Snow Lake, and at Sherridon; the lower $\delta^{34}S$ values at Sherridon may reflect the influence of reduced sedimentary rocks in the mine sequence.

Table 7. Pb isotope ratios of galena from different ore types of the Lalor massive sulphide deposit.

Sample	Description	Location (Ore Type)	$^{206}Pb/^{204}Pb$	$^{207}Pb/^{204}Pb$	$^{208}Pb/^{204}Pb$
SD-524	Euhedral grains with minor pyrite and pyrrhotite in a matrix of quartz and chlorite (DUB252W01, 1016.8 m)	25 Lens (Type 3)	15.403	15.12	34.899
SD-581	12 cm thick vein of pyrrhotite, pyrite, and galena with minor chalcopyrite in quartz- biotite-actinolite/ tremolite-garnet (DUB258W01, 803.7 m)	N/A (vein)	15.402	15.128	34.892
SD-611	Vein of sphalerite and galena with minor chalcopyrite in quartz-muscovite-gahnite-biotite (DUB169, 900.5 m)	21 Lens (Type 3)	15.399	15.113	34.888
SD-652	Coarse pyrite and sphalerite with lesser galena in actinolite-tremolite and epidote (DUB211, 909.2 m)	10 Lens (Type 3)	15.398	15.125	34.898
SD-654	Coarse pyrite and galena with interstitial sphalerite in carbonate (DUB174, 877.8 m)	31 Lens (Type 1)	15.396	15.122	34.885
SD-655	Galena adjacent to quartz vein in a massive pyrite (underground, 825 mL)	10 Lens (N/A)	15.394	15.116	34.868
SD-662	Thick (50 cm) galena vein cutting stringer zone sulphides (underground, 810 mL)	10 Lens (vein)	15.396	15.122	34.891
SD-663	Quartz vein with galena concentrated in a fold hinge (underground, 865 mL)	20 Lens (vein)	15.412	15.132	34.936

deposits to have a very narrow range of values, reflecting probable loss of light sulphur during recrystallization (Crowe, 1994; Cook and Hoefs, 1997). In contrast, shear zone-hosted orogenic gold deposits in the Flin Flon-Snow Lake belt have generally higher $\delta^{34}S$ values (2.8 to 5.5‰: Fedorowich et al., 1991; Ansdell and Kyser, 2006), consistent with hydrothermal fluids in the shear zones interacting with a wide range of Proterozoic metamorphic and igneous rocks. The data also contrast with the $\delta^{34}S$ values of barren sulphide occurrences in rocks of similar age and metamorphic grade but outside the Flin Flon-Snow Lake belt (e.g. Polito et al., 2007).

Lead isotope ratios were measured on 6 galena separates from the Au-Ag-Pb-Cu mineralization associated with chlorite-carbonate-altered rocks and 3 galena separates from the massive sulphides in the 10 and 11 lenses (Table 7). All samples exhibit a tight cluster of $^{206}Pb/^{204}Pb$, $^{207}Pb/^{204}Pb$, and $^{208}Pb/^{204}Pb$ ratios, averaging 15.400, 15.122, and 34.895, respectively, with no difference between the ore types. These data compare closely to the Pb-isotope ratios of galena separates from Chisel and Chisel North (15.432, 15.161, and 35.058: Thorpe, 2008) at low $^{206}Pb/^{204}Pb$ and $^{207}Pb/^{204}Pb$ (Fig. 9). The similarity of Pb isotope compositions of galena in the Au-Ag-Pb-Cu galena-sulphosalts-chalcopyrite mineralization and in the massive sulphides strongly suggests a common Pb source and negates a late-stage post-magmatic event as the origin of the Au-Ag-Pb-Cu mineralization. A post-magmatic event would have been expected to introduce distinctly different and likely more radiogenic Pb (cf. Sangster, 1972, 1978; Thorpe, 2008), similar to that in the nearby New Britannia (Nor Acme), Rex, Herb

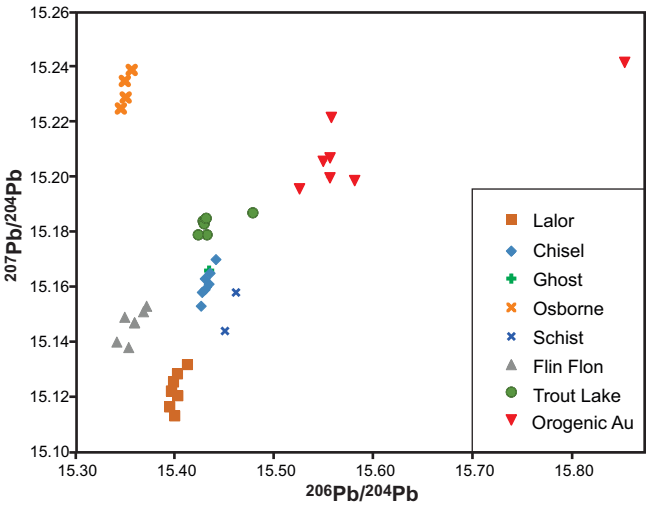

Figure 9. Bivariate plot of $^{207}Pb/^{204}Pb$ versus $^{206}Pb/^{204}Pb$ ratios for galena from selected volcanogenic massive sulphide (VMS) deposits and orogenic Au deposits in the Flin Flon-Snow Lake belt. Data are from Thorpe (2008) and J.M. Franklin (unpublished). The samples were collected by D. Sangster, J.M. Franklin, A. Galley, M. Fedikow, and R. Healy, and the analyses were performed in a number of different laboratories, including at the University of Alberta (G.L. Cumming, 1982), Geospec Consultants Limited, and at the Geological Survey of Canada. Data for late post-magmatic mineralization are from orogenic Au deposits: Nor Acme (New Britannia), Bingo, Ferro, Herb lake, Rex Mine, and Threehouse. Data for Lalor are from this study. The Pb isotopic compositions of galena from Lalor are the least radiogenic of the VMS deposits in the region, but generally fall on a Pb-isotope linear array including the Lalor, Ghost, and Chisel deposits. Galena lead isotope signatures for the younger, orogenic Au deposits of the Snow Lake camp (Nor Acme-New Britannia, Rex, Herb Lake, Bingo, and Ferro) form a distinctly separate secondary array.

Lake, Bingo, and Ferro Au deposits of the Snow Lake camp (Fig. 9).

Lalor ore galena is the least radiogenic of the VMS deposits in the region but generally falls on the Pb-isotope linear array of the Flin Flon-Snow Lake mineral belt (cf. Sangster 1972, 1978). The linear array of data on the Pb-Pb plot is similar to that inferred for crust-mantle mixing in other Precambrian greenstone terranes (e.g. Thorpe, 1999) and reflects contributions of both older crustal components and mantle sources. The most radiogenic end-members represent the signatures of material derived from the crust.

SUMMARY AND CONCLUSIONS

Four major ore types are recognized in the 12 ore lenses at Lalor, including Fe-Zn-rich massive sulphides, Au-Cu rich semi-massive and stockwork-like chalcopyrite in chloritic rocks (dominated by chlorite-biotite-staurolite-anthophyllite-cordierite ± kyanite/sillimanite), Au-Ag-Pb-Cu disseminated sulphides and sulphosalts in chlorite-carbonate-actinolite (dominated by chlorite-calcite ± diopside ± epidote ± talc), and pyritic quartz-biotite rock. In the Fe-Zn-rich massive sulphides, Au is interstitial to pyrite and sphalerite in coarsely recrystallized polycrystalline aggregates, commonly with sulphosalts and chalcopyrite. In semi-massive and stockwork-like Cu-Au mineralization Au is closely associated with chalcopyrite, and in chlorite-carbonate-actinolite ± calc-silicate rocks Au is associated with disseminated polymetallic sulphides, especially galena, and related Ag-Sb-Pb-sulphosalts.

All ores have been extensively recrystallized during syn-D_2 amphibolite-facies metamorphism. The stoichiometric compositions of the major Cu-Fe-sulphides (pyrite, pyrrhotite, chalcopyrite), the very uniform composition of sphalerite, the low trace-element contents in galena, and the abundance of minor and trace sulphosalts and other minerals are typical of massive sulphide ores that have been extensively recrystallized (e.g. Chen and Petruk, 1980; Petruk and Schnarr, 1981; Craig and Vokes, 1993; Petruk and Wilson, 1993; Huston et al., 1995). In such ores, trace elements in the major ore minerals are expelled during recrystallization to form minor phases that commonly occur at the margins of the grains or at triple-junction contacts. The presence of mercurian gold probably reflects the loss of Hg from primary sphalerite during metamorphism and its collection by electrum (cf. Healy and Petruk, 1988), a major source of Hg in all of the deposits of the belt (e.g. Healy and Petruk, 1990). Certain minerals, such as tetrahedrite, retain their high Ag contents despite the metamorphism. In some metamorphosed ore deposits, pyrite decomposition liberates sulphur that may play a role in remobilization of Au (e.g. as $Au(HS)_2^-$ in metamorphic hydrothermal fluids derived from dehydration reactions), and high fS_2 conditions caused by pyrite breakdown have been documented at several highly metamorphosed massive sulphide deposits, such as Osborne Lake, Montauban, and Geco (Bristol and Froese, 1989; Tomkins et al., 2006; Tomkins 2007). However, strong buffering by iron silicates or oxides may limit this process, and the uniformly high FeS contents of sphalerite at Lalor suggest that fS_2 remained low during metamorphism (e.g. Craig and Vokes, 1993). Thus, although soft and ductile minerals like galena, various sulphosalts, electrum, and gold were mechanically remobilized into fractures and cleavages, metamorphic reactions that might have dissolved (and transported) Au likely did not occur.

The ore lenses also preserve an apparent primary metal enrichment. Zn-rich massive sulphide ores are Cd-, Hg-, Sb-, and As-rich, whereas the Cu-rich semi-massive sulphide and stockwork ores (normalized to 100% sulphides) are enriched in Co, Ni, Mo, Se, Te, ±Bi. The Pb-rich ores are enriched in Au, Ag, As, Se, and Te compared to the other ore types. In general, Au shows a generally poor correlation with all other trace elements, except Ag. As in other deposits of the Chisel Sequence, high Au grades occur in both Cu- and Zn-rich ores in different lenses, and this most likely reflects primary differences in the conditions of Au mineralization (e.g. including both high-temperature Cu-Au mineralization and lower temperature Zn-Au mineralization (Huston, 2000).

The unusual stratigraphic position of the Pb-rich ores relative to the other ore lenses at Lalor raises the possibility that they are not part of the VMS system but were emplaced during a much later metamorphic event. However, the tight clustering of the Pb-isotope data along the Flin Flon-Snow Lake linear array suggests that the Pb and the closely associated Au were cogenetic with the massive sulphides. As noted by Sangster (1978), the fact that the galena from the various VMS deposits cluster and do not lie on secondary isochrons, like the Au deposits, suggests that the Pb (and by inference other metals) in each deposit have a discrete uniform composition and do not show any multi-stage post-magmatic history. The presence of "low-temperature" disseminated galena-rich ores stratigraphically below the main massive sulphide lenses suggests that they formed as a late-stage synvolcanic hydrothermal overprint, possibly in response to subseafloor boiling. Galley et al. (1993) and Gibson et al. (2014) similarly interpret the Chisel, Lost, and Ghost deposits as having formed within a shallow marine basin in which boiling of the hydrothermal fluid likely occurred, and Engelbert et al. (2014b) proposes boiling as the probable mechanism of formation of the high-grade Au ores at Photo Lake. Such low-temperature, disseminated-style ore assemblages at Lalor are

Table 8. Trace element contents of different ore types from Lalor (normalized to 100% sulphides) compared to Snow Lake mineral concentrates.

Deposit	Concentrate/ Ore	(n)	Cu	Fe	Zn	Pb	Au	Ag	As	Sb	Co	Se	Ni	Cd	Mo	Te	Bi	Hg	Tl	Ga	In	Sn
			wt.%				ppm															
Lalor	Fe-Zn	23	5.08	17	24.9	0.34	4.39	110	768	181	208	273	48	648	11	30	1	180	0.3	19	2	24
Lalor	Cu-Au	6	29.1	20.4	7.93	0.19	86.15	362	91	15	342	533	77	219	18	142	15	24	0.8	65	3	75
Lalor	Au-Ag-Pb	15	7.69	13.3	24.4	10.1	38.21	563	314	38	294	778	41	625	17	140	8	82	0.9	88	2	80
Lalor	Low-sulphide	5	16	15	3.16	0.49	66.61	401	464	3	901	824	90	155	16	117	4	12	0.5	64	2	23
Snow Lake	Cu concentrate	3	19.5	34.6	2.16	0.03	5.91	93	655	367	381	225	21	57	29	63	29	16	0.6	12	30	16
Stall/Rod	Cu Concentrate	3	19.6	34.4	1.36	0.02	6.16	37	472	49	297	255	16	40	22	52	41	10	0.2	7	29	12
Chisel	Cu Concentrate	3	19.7	22.2	9.73	6.21	21	1800	2042	3379	38	293	24	250	28	46	55	73	4.7	5	9	26
Snow Lake	Zn Concentrate	3	0.71	9.61	53.7	0.02	0.52	30	353	78	17	116	<10	1300	2	4	2	120	0.5	11	8	9
Chisel	Zn Concentrate	4	0.22	8.42	54.5	0.2	0.22	27	585	56	20	83	10	1300	2	3	2	120	0.4	10	6	8
Chisel	Pb Concentrate	3	1.21	6.86	6.29	61.4	8.03	956	2229	8436	8	589	24	120	8	120	200	130	26	2	1	6

Lalor data are calculated from samples in Table 5, after normalizing to 100% metals+Fe+S. Type 1 includes only samples with Me+Fe+S >30 wt%; Au, Ag, and Te concentrations in the calculations were cut-off at 30 ppm Au, 300 ppm Ag, and 150 ppm Te. Data for mill concentrates from other Snow Lake deposits are from Hannington and Jonasson, 1986, unpublished data.

also much more sensitive to metamorphism and remobilization, perhaps explaining why part of the Au-Ag-Pb-Cu ore is spatially associated with highly strained rocks, brittle amphibolitic assemblages, and weakly altered mafic dykes (Caté et al., 2015).

The ores at Lalor are geochemically and mineralogically similar to the other deposits of the Chisel Sequence (Chisel, Chisel North, Lost, and Ghost). Gold is significantly enriched in all of the deposits compared to the Anderson Sequence (Stall, Rod, and Anderson). Silver, As, Cd, Hg, and Sn contents (normalized to 100% sulphides) are also higher than in typical Snow Lake concentrates (M. Hannington and I. Jonasson, unpublished; Table 8). Notably, the Co, Se, Ni, and Te abundances in the Lalor ore-related minerals are significantly higher than those in the Chisel ores. Trace Co and Ni occur in pyrrhotite and pyrite, and cobaltite, gudmundite, and Se-bearing arsenopyrite are present in the massive sulphides. These differences may reflect the dominantly mafic host rocks and the lack of rhyolite at Lalor compared to Chisel. The most Au-rich deposits of the Chisel Sequence show a close association with felsic volcanic rocks and local rhyolite domes (Galley et al., 1993; Gibson et al., 2014). Similarly, the Au-rich Photo Lake deposit has been interpreted to occur within a thick section of coherent rhyolite (Engelbert et al., 2014a). Although the Lalor deposit is thought to be situated at a similar stratigraphic position as Chisel and Chisel North (Bailes et al., 2013), detailed studies suggest some differences between the footwall successions (Bailes et al., 2013; Caté et al., 2013a,b, 2015), including a minor proportion of felsic volcanic rocks in the Lalor volcanic (footwall) succession. Moreover, mafic magmatism was clearly ongoing during the mineralizing event at Lalor, as evidenced by the presence of dykes with compositions similar to the Threehouse basalt. These observations indicate that Au enrichment in the camp is not limited to deposits that have mainly rhyolite in the immediate footwall.

ACKNOWLEDGEMENTS

We thank Hudbay Minerals Inc. and the Manitoba Geological Survey, in particular, A. Bailes, S. Bernauer, C. Böhm, S. Gagné, B. Janser, J. Levers, D. Simms, T. Schwartz and C. Taylor, who provided access to the mine and core and insightful discussions on the Lalor deposit. H. Gibson, B. Lafrance, D. Tinkham, J. Lam, and M. Englebert of the Laurentian University Snow Lake research group shared knowledge of the Snow Lake district and VMS systems. The senior author was funded jointly by Hudbay Minerals and by the Geological Survey of Canada through the RAP program. We thank Jan Peter for reviews and editorial handling.

REFERENCES

Ansdell, K.M. and Kyser, K.T., 2006. Mesothermal gold mineralization in a Proterozoic greenstone belt, western Flin Flon Domain, Saskatchewan, Canada; Economic Geology, v. 87, p. 1496–1524.

Bailes, A.H., 2008. Geological setting of the Lalor and Photo Lake VMS deposits; Hudbay Internal Report, Bailes Geoscience, 45 p.

Bailes, A.H., 2009. Geological and Geochemical Investigation of Altered Rocks Hosting the Lalor VMS Deposit; Unpublished Report for HudBay Minerals Inc., 96 p.

Bailes A.H., 2011. A review of structural features associated with VMS deposits in the Chisel-Lalor-Photo lakes area; Unpublished Report for HudBay Minerals Inc., 31 p.

Bailes, A.H. and Galley, A.G., 1996. Setting of Paleoproterozoic volcanic-hosted massive sulphide deposits, Snow Lake, *In:* EXTECH I: A Multidisciplinary Approach to Massive Sulphide Research in the Rusty Lake and Snow Lake Greenstone Belts, Manitoba, (ed.) G.F. Bonham-Carter, A.G. Galley and G.E.M. Hall; Geological Survey of Canada, Bulletin 426, p.105–138.

Bailes, A.H. and Galley, A.G., 1999. Evolution of the Paleoproterozoic Snow Lake arc assemblage and geodynamic setting for associated volcanic-hosted massive sulphide deposits, Flin

Flon Belt, Manitoba, Canada; Canadian Journal of Earth Sciences, v. 36, no. 11, p. 1789–1805. doi:10.1139/e98-111

Bailes, A., Rubingh, K., Gagné, S., Taylor, C., Galley, A., Bernaeur, S., and Simms, D., 2013. Volcanological and structural setting of Paleoproterozoic VMS and Gold deposits at Snow Lake, Manitoba; Geological Association of Canada–Mineralogical Association of Canada Joint Annual Meeting, Winnipeg, Manitoba, May 2013, Field Trip Guidebook FT-A2, Manitoba Innovation, Energy and Mines, Manitoba Geological Survey Open File OF2013-3, 63 p.

Barton, P.B. and Bethke, P.M. Jr., 1987. Chalcopyrite disease in sphalerite: Pathology and epidemiology; American Mineralogist, v. 72, p. 451–467.

Bristol, C.C. and Froese, E., 1989. Highly metamorphosed altered rocks associated with the Osborne Lake volcanogenic massive sulfide deposit, Snow Lake area, Manitoba; Canadian Mineralogist, v. 27, p. 593–600.

Caté, A., Mercier-Langevin, P., Ross, P.-S., Duff, S., Hannington, M.D., Dubé, B., and Gagné, S., 2015. Geology and Au enrichment processes at the Paleoproterozoic Lalor auriferous volcanogenic massive sulphide deposit, Snow Lake, Manitoba, *In:* Targeted Geoscience Initiative 4: Contributions to the Understanding of Volcanogenic Massive Sulphide Deposit Genesis and Exploration Methods Development, (ed.) J.M. Peter and P. Mercier-Langevin; Geological Survey of Canada, Open File 7853, p. 131–145.

Caté, A., Mercier-Langevin, P., Ross, P.-S., Duff, S., Hannington, M., Dubé, B., and Gagné, S., 2013a. The Paleoproterozoic Lalor VMS deposit, Snow Lake, Manitoba: preliminary observations on the nature and architecture of the gold- and base metal-rich ore and alteration zones; Geological Survey of Canada, Open File 7483, 19 p.

Caté, A., Mercier-Langevin, P., Ross, P.-S., Duff, S., Hannington, M., Dubé, B., and Gagné, S., 2013b. Preliminary observations on the geological environment of the Paleoproterozoic auriferous volcanogenic massive sulphide deposit of Lalor, Snow Lake, Manitoba; Geological Survey of Canada, Open File 7372, 13 p.

Caté, A., Mercier-Langevin, P., Ross, P.-S., and Simms, D., 2014a. GS-8 Structural controls on geometry and ore distribution in the Lalor auriferous VMS deposit, Snow Lake, west-central Manitoba (part of NTS 63K16): preliminary results from underground mapping, *In:* Report of Activities 2014; Manitoba Mineral Resources, Manitoba Geological Survey, p. 104–115.

Caté, A., Mercier-Langevin, P., Ross, P.-S., Duff, S., Hannington, M., Gagné, S., and Dubé, 2014b. Insights on the chemostratigraphy of the volcanic and intrusive rocks of the Lalor auriferous volcanogenic massive-sulphide deposit host succession, Snow Lake, Manitoba; Geological Survey of Canada, Current Research 2014-6, 20 p.

Chen, T.T. and Petruk, W., 1980. Mineralogy and characteristics that affect recoveries of metals and trace elements from the ore at Heath Steele Mines, New Brunswick; Canadian Institute of Mining and Metallurgy Bulletin v. 73, p. 167–178.

Cook, N.J. and Hoefs, J., 1997. Sulphur isotope characteristics of metamorphosed Cu-(Zn) volcanogenic massive sulfide deposits in the Norwegian Caledonides; Chemical Geology, v. 135, p. 307–324.

Corriveau, L. and Spry, P.G., 2014. Metamorphosed hydrothermal ore deposits, *In:* Geochemistry of Mineral Resources, Treatise on Geochemistry, (ed.) S.D. Scott; Elsevier, New York, v. 12.

Craig, J.R., Vokes, F.M., and Simpson, C., 1991. Rotational fabrics in pyrite from Ducktown, Tennessee; Economic Geology, v. 86, p. 1737–1746.

Craig, J.R. and Vokes, F.M., 1993. The metamorphism of pyrite and pyritic ores: an overview; Mineralogical Magazine, v. 57, p. 3–18.

Crowe D.E., 1994. Preservation of original hydrothermal $\delta^{34}S$ values in greenschist to upper amphibolite volcanogenic massive sulfide deposits; Geology, v. 22, p. 873–876.

Engelbert, M.S., Friesen, V., Gibson, H., and Lafrance, B., 2014a. Volcanic reconstruction of the productive VMS ore interval in the Paleoproterozoic Chisel sequence, Snow Lake, Manitoba, *In:* Program with Abstracts; Geological Association of Canada–Mineralogical Association of Canada Joint Annual Meeting, Fredericton, May 22–22, 2014, p. 83–84.

Engelbert, M.S., Gibson, H.L., and Lafrance, B., 2014b. Geologic Setting, Mineralogy, and Geochemistry of the Paleoproterozoic Photo Lake VMS Deposit, Snow Lake, Manitoba; PDAC-SEG Student Minerals Colloquium, March 3, (poster presentation).

Fedorowich, J., Stauffer, M., and Kerrich, R., 1991. Structural setting and fluid characteristics of the Proterozoic Tartan Lake gold deposit, Trans-Hudson Orogen, northern Manitoba; Economic Geology, v. 86, p. 1434–1467.

Gagné, S., Beaumont-Smith, C.J., Williams-Jones, A.E., and Hynes, A., 2007. Investigation of a Pb-Ag-Au–rich hanging-wall in lens 4 of the Chisel North mine, Snow Lake, Manitoba (NTS 63K16): preliminary results, *In:* Report of Activities 2007; Manitoba Science, Technology, Energy and Mines, Manitoba Geological Survey, p. 43–50.

Galley, A.G., Syme, R., and Bailes, A.H., 2007. Metallogeny of the Paleoproterozoic Flin Flon Belt, Manitoba and Saskatchewan, *In:* Mineral Deposits of Canada: A Synthesis of Major Deposit Types, District Metallogeny, the Evolution of Geological Provinces, and Exploration Methods, (ed.) W.D. Goodfellow; Geological Association of Canada, Mineral Deposits Division, Special Publication 5, p. 509–531.

Galley, A.G., Bailes, A.H., and Kitzler, G., 1993. Geological setting and hydrothermal evolution of the Chisel Lake and North Chisel Zn–Pb–Cu–Ag–Au massive sulphide deposits, Snow Lake, Manitoba; Exploration and Mining Geology, v. 2, p. 271–295.

Gibson, H., Engelbert, M.S., Lafrance, B., Friesen, V., DeWolfe, M., Tinkham, D.K., and Bailes, A.H., 2014. Reconstruction of the ore interval and environment for the Paleoproterozoic Lost and Ghost Lake VMS deposits, Snow Lake, Manitoba; *In:* Program with Abstracts; Geological Association of Canada-Mineralogical Association of Canada Joint Annual Meeting, Fredericton, May 22–22, 2014, p. 102.

Healy, R.E. and Petruk, W., 1988. Mineralogical characteristics that affect metal recoveries from Cu, Zn, Pb and Ag ores of Manitoba: An Investigation of the mineralogy of the Trout Lake deposit; Canada Centre for Minerals and Energy Technology, Investigative Report IR 88-61, 181 p.

Healy, R.E. and Petruk W., 1990. Petrology of Au-Ag-Hg alloys and 'invisible' gold in the Trout Lake massive sulfide deposit, Flin Flon, Manitoba; Canadian Mineralogist, v. 28, p.189–206.

HudBay Minerals Inc., 2014, Lalor operation webpage, http://www.hudbayminerals.com/English/OurBusiness/Operations/Lalor/default.aspx

Huston, D.L., Sie, S.H., Suter, G.F., Cooke, D.R., and Both, R.A., 1995. Trace elements in sulfide minerals from eastern Australian volcanic-hosted massive sulfide deposits: Part I. Proton microprobe analyses of pyrite, chalcopyrite, and sphalerite, and Part II. Selenium levels in pyrite: comparison with $\delta^{34}S$ values and implications for the source of sulfur in volcanogenic hydrothermal systems; Economic Geology, v. 90, p. 1167–1196.

Huston, D.L., 2000. Gold in volcanic-hosted massive sulfide deposits: distribution, genesis, and exploration, *In:* Gold in 2000, (ed.) S.G. Hagemann and P.E. Brown; Reviews in Economic Geology, v. 13, p. 400–426.

Kraus, J. and Williams, P.F., 1999. Structural development of the Snow Lake allochthon and its role in the evolution of the southeastern Trans-Hudson Orogen in Manitoba, central Canada; Canadian Journal of Earth Sciences, v. 36, p. 1881–1899.

Lam, J., Tinkham, D.K., and Gibson, H., 2013. Identification of metamorphic assemblages and textures associated with gold mineralization at the Lalor deposit, Snow Lake, Manitoba, *In:* Program with Abstracts; Geological Association of Canada–Mineralogical Association of Canada Joint Annual Meeting, Winnipeg, May 22–24, 2013, p. 127.

Lam, J., Tinkham, D.K., and Gibson, H., 2014. Characterization of gold occurrences with respect to metamorphism at the Lalor deposit, Snow Lake, Manitoba, *In:* Program with Abstracts; Geological Association of Canada–Mineralogical Association of Canada Joint Annual Meeting, Fredericton, May 22–22, 2014, p. 150–151.

Martin, P., 1966. Structural analysis of Chisel Lake orebody; Canadian Mining and Metallurgical Bulletin, v. 69, p. 208–214.

Menard, T. and Gordon, T.M., 1997. Metamorphic P-T paths from the eastern Flin Flon belt and Kisseynew domain, Snow Lake, Manitoba; Canadian Mineralogist, v. 35, p. 1093–1115.

Mercier-Langevin, P., Caté, A., and Ross, P.-S., 2014. GS-7 Whole-rock oxygen-isotope mapping of the footwall alteration zones at the Lalor auriferous VMS deposit, Snow Lake, west-central Manitoba (NTS 63K16), *In:* Report of Activities 2014; Manitoba Mineral Resources, Manitoba Geological Survey, p. 94–103.

Petruk, W. and Schnarr, J.R., 1981. An evaluation of the recovery of free and unliberated mineral grains, metals and trace elements in the concentrator of Brunswick Mining and Smelting Corp. Ltd.; Canadian Institute of Mining and Metallurgical Bulletin, v. 74, p. 132–159.

Petruk, W. and Wilson, J.M., 1993. Silver and gold in some Canadian volcanogenic base metal deposits, *In:* Proceedings, (ed.) Maurice, Y.T.; 8th Quadrennial IAGOD Symposium, Schweizerbart'sche, Stuttgart, p. 105–117.

Polito P., Kyser, K., Lawie, D., Cook, S., and Oates, C., 2007. Application of sulphur isotopes to discriminate Cu-Zn VHMS mineralization from barren Fe sulphide mineralization in the greenschist to granulite facies Flin-Flon - Snow Lake - Hargrave River region; Geochemistry, Exploration, Analysis, Environment, v. 7, p. 129–138.

Sangster D.F., 1972. Isotopic Studies of Ore-Leads in the Hanson Lake - Flin Flon - Snow Lake Mineral Belt, Saskatchewan and Manitoba; Canadian Journal of Earth Sciences, v. 9, p. 500–513.

Sangster, D.F., 1978. Isotopic studies of ore-leads of the circum-Kisseynew volcanic belt of Manitoba and Saskatchewan; Canadian Journal of Earth Sciences, v. 15, p. 1112–1121.

Shanks, W.C., 2001. Stable Isotopes in Seafloor Hydrothermal Systems: Vent fluids, hydrothermal deposits, hydrothermal alteration, and microbial processes; Reviews in Mineralogy and Geochemistry, v. 43, p. 468–525.

Tinkham, D.K., 2013. A model for metamorphic devolatilization in the Lalor deposit alteration system, Snow Lake, Manitoba, *In:* Program with Abstracts; Geological Association of Canada–Mineralogical Association of Canada Joint Annual Meeting, Winnipeg, May 22–24, 2013, p. 187.

Thorpe, R.I., 1999. The lead isotope linear array for volcanogenic massive sulfide deposits of the Abitibi and Wawa subprovinces, Canadian Shield, *In:* The Giant Kidd Creek Volcanogenic Massive Sulfide Deposit, Western Abitibi Subprovince, Canada, (ed.) M.D. Hannington and C.T. Barrie; Society of Economic Geologisst, Monograph 10, p. 555– 576.

Thorpe, R.I., 2008. Release of lead isotope data in 4 databases: Canadian, western Superior, foreign, and whole rock and feldspar; Geological Survey of Canada, Open File Report 5664, 42 p.

Tomkins, A.G., 2007. Three mechanisms of ore re-mobilisation during amphibolite facies metamorphism at the Montauban Zn-Pb-Au-Ag deposit; Mineralium Deposita, v. 42, p. 627–637.

Tomkins, A.G., Frost, R.B., and Pattison, D.R.M., 2006. Arsenopyrite melting during metamorphism of sulfide ore deposits; Canadian Mineralogist, v. 44, p. 1045–1062.

Zaleski, E., Froese, E., and Gordon, T. M., 1991. Metamorphic petrology of Fe-Zn-Mg-Al alteration at the Linda volcanogenic massive sulfide deposit, Snow Lake, Manitoba; Canadian Mineralogist, v. 29, p. 995–1017.